

PLASMONS AND SURFACE PLASMONS IN BULK METALS, METALLIC CLUSTERS, AND METALLIC HETEROSTRUCTURES

R. v. Baltz
Institut für Theorie der Kondensierten Materie
Universität Karlsruhe
D-76128 Karlsruhe, Germany

ABSTRACT

This article gives an introduction and survey in the theory and spectroscopy of plasmons in the bulk, as well as on boundaries of metals. First, concepts to describe the metallic state and its interaction with electromagnetic fields are summarized, then various approaches to obtain the plasmon–dispersion relations are studied. Finally, some actual questions such as correlation effects and the surface charge density profile on the plasmon–dispersion are discussed.

I. INTRODUCTION

Plasmons are quantized wave-like excitations in a plasma, i.e. a system of mobile charged particles which interact with one another via the Coulomb forces. The classical example is an ionized gas consisting of (positive) ions and (negative) electrons in a discharge tube. In metals (and in some highly doped semiconductors, too) the electrons likewise form a plasma. In contrast to the aforementioned example, however, the electrons form a degenerate Fermi-system, i.e. even at low temperature, the electrons have a large kinetic energy (\approx Fermi-energy) so that (room-) temperature has little influence on the electronic excitations. The ions, on the other hand, because of their large mass have little kinetic energy and their (crystal-) structure and collective excitations (=phonons) are completely dominated by the electrons.

As a consequence of the long range nature of the Coulomb interaction the frequency of the plasma oscillations,

$$\omega_p = \sqrt{\frac{n_0 e^2}{m_0 \epsilon_0}} \quad (1)$$

is very high compared with other collective excitations like phonons. n_0 is the density and m_0 is the (free-) electron mass. For example, in *Al* we have $\hbar\omega_p = 15\text{eV}$, whereas, typical phonon energies are in the 10meV range. For a survey, see Di Bartolo's article in this book.

Collective excitations in classical plasmas were first studied by Langmuir [1]. The pioneering theoretical investigations on their quantum counterparts were carried-out by Bohm and Pines, see Pines [2]. Experimental evidence for the existence of plasmons as a well defined collective mode of the valence electrons of metals comes from characteristic energy-loss experiments. In such an experiment, one measures the energy loss–spectrum of keV electrons transmitted through a thin metallic foil, Fig. 1. The multiple excitation of this mode is also direct evidence for the quantization of the plasmon energy in units of $\hbar\omega_p$.

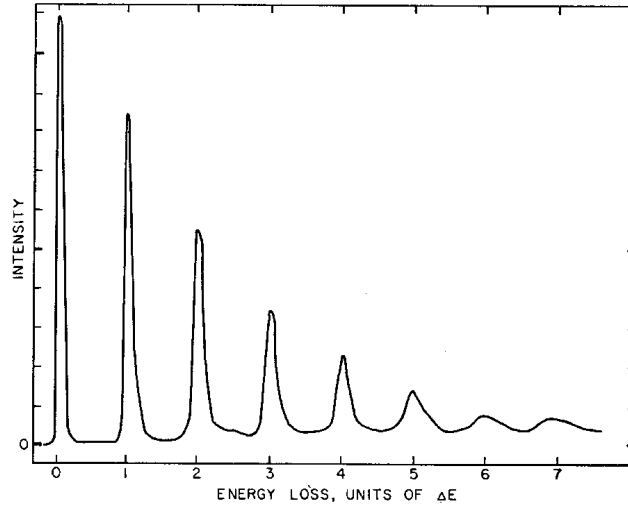


Figure 1. Electron-energy-loss spectrum for a beam of 20keV electrons passing through an Al foil of 2580\AA thickness. $\Delta E = \hbar\omega_p = 15\text{eV}$. From Marton *et al.* [3]

Excellent books and reviews on the theory and spectroscopy of solid state plasmas are available. In particular we recommend Pines and Nozieres [4], Platzman and Wolf [5], and DiBartolo [6]. Electron-energy-loss-plasmon spectroscopy became a major tool to study electronic excitations in solids, for surveys see Raether [7], Schnatterly [8], and Fink [9].

II. CONCEPTS TO DESCRIBE THE METALLIC STATE

II. A. The Standard Model: Jellium

To describe the characteristic metallic properties like the groundstate energy, the elementary excitations, and the interaction with electromagnetic fields, simple models have been found which are of immense value to solid state physics. For an introduction see e.g. Pines[2] or Ashcroft and Mermin [10].

The simplest quantum mechanical model of the metallic state is due to Sommerfeld. The Coulomb interactions between electrons as well as with the ions are completely neglected, yet the many particle aspect is taken into account. The single-electron states are plane-waves with wave-number \mathbf{k} and energy $\epsilon_{\mathbf{k}}$ which - in accordance with the Pauli-principle - will be “filled” in \mathbf{k} -space up to the radius k_F , the Fermi-wave number.

single particle states:

$$|\mathbf{k}\rangle = \exp(i\mathbf{k}\mathbf{r})$$

$$\epsilon(\mathbf{k}) = (\hbar\mathbf{k})^2/2m_0$$

Fermi ground state:

$$k_F = (3\pi^2 n)^{1/3}$$

$$\epsilon_F = (\hbar k_F)^2/2m_0$$

$$v_F = \hbar k_F/m_0$$

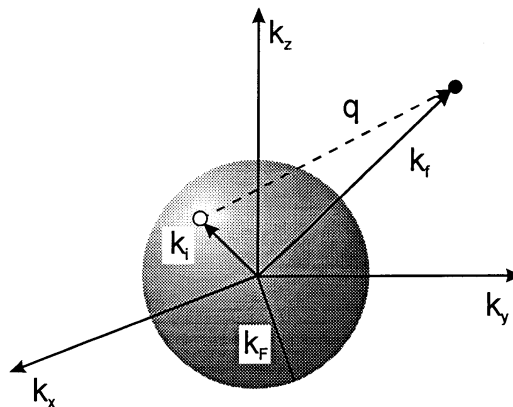


Figure 2. Momentum distribution of the noninteracting Fermi-gas at zero temperature. In addition, a particle-hole excitation from initial state \mathbf{k}_i to final unoccupied state \mathbf{k}_f is shown.

<i>El</i>	<i>Z</i>	$n/\text{\AA}^3$	r_s	$k_F/\text{\AA}$	ϵ_F/eV	$\hbar\omega_p/\text{eV}$	m^*/m_0	ϵ_∞	<i>Ref</i>
<i>Li</i>	1	0.0470	3.25	1.12	4.74	7.10	2.30	1.02	[7,10]
<i>Na</i>	1	0.0265	3.93	0.92	3.24	5.75	1.30	1.06	[10,15]
<i>K</i>	1	0.0140	4.86	0.75	2.12	3.80	1.20	1.15	[10,15]
<i>Rb</i>	1	0.0115	5.20	0.70	1.85	3.40	1.30	1.25	[10,15]
<i>Cs</i>	1	0.0091	5.62	0.65	1.59	2.90	1.50	1.29	[10,15]
<i>Ag</i>	1	0.0586	3.02	1.20	5.49	3.78	1.10		[7,10]
<i>Be</i>	2	0.2470	1.87	1.94	14.3	19.0	0.42	1.02	[7,10]
<i>Mg</i>	2	0.0861	2.66	1.36	7.08	10.5	1.30	1.01	[7,10]
<i>Al</i>	3	0.1810	2.07	1.75	11.7	15.0	1.40	1.11	[7,10,15]

Tab.1. Parameters for some selected metallic elements and compounds. $\epsilon_\infty = 1 + 4\pi n\alpha$ where α is the polarizability of the ions. For *Ag* ϵ_∞ shows a strong dispersion peak at ω_p . Experimental data for m^* contain electron-electron and electron-phonon renormalization contributions and are, thus, larger than the bandstructure mass which is needed in (1).

Next, we consider the influence of the Coulomb interaction between the electrons and the ions. For the “simple” metals - which include the alkalis, *Al*, *Ga*, *In*, *Be*, and *Mg* - the crystal potential is weak so that it is a good approximation to smear-out the ions into a positive background charge density $\rho_+ = -en_0$: Jellium. To describe the strength of the Coulomb interaction we compare the average kinetic and potential energy per electron *

$$\epsilon_{kin} = \frac{3}{5}\epsilon_F, \quad \epsilon_{pot} \approx \frac{e^2}{4\pi\epsilon_0} \langle \frac{1}{r} \rangle, \quad (2)$$

where $\langle r \rangle \approx n^{-1/3}$ is the mean electron distance. It is convenient to use “atomic units”, i.e. we measure the lengths in units of Bohr-radii, energies in Rydbergs and characterize the density by the dimensionless Wigner-Seitz radius r_s .

$$\text{atomic units: } \begin{cases} \text{Bohr-radius:} & a_B = 4\pi\epsilon_0\hbar^2/m_0e^2 = 0.529\dots\text{\AA} \\ \text{Rydberg-energy:} & R_y = e^2/8\pi\epsilon_0a_B = 13.56\dots\text{eV} \\ r_s\text{-parameter:} & n^{-1} = \frac{4\pi}{3}(a_B r_s)^3 \end{cases} \quad (3)$$

As $\epsilon_{pot} \propto r_s^{-1}$ but $\epsilon_{kin} \propto r_s^{-2}$, the Coulomb interaction becomes weak in the high density limit, $r_s < 1$. In most cases, however, r_s is not small but usually lies in the range 2.6, Tab. 1.

The Hamiltonian of Jellium is given by

$$\hat{\mathbf{H}} = \sum_{j=1}^N \frac{\hat{\mathbf{p}}_j^2}{2m_0} + \frac{1}{2} \sum_{i \neq j} \frac{e^2}{4\pi\epsilon_0} \frac{1}{|\hat{\mathbf{r}}_i - \hat{\mathbf{r}}_j|} + \hat{\mathbf{H}}_{el-ion} + \hat{\mathbf{H}}_{ion-ion} \quad (4)$$

The Coulomb interaction couples the states of all particles so that the exact eigenstates of $\hat{\mathbf{H}}$ are not analytically accessible, yet reasonable approximations have been found. Owing to the uniform background charge the average field acting on one electron vanishes, so that as a first guess one might use a product of plane waves in accordance with the exclusion principle - up to k_F one electron per \mathbf{k} and spin. This is the Hartree-approximation, which, gives the same result for the ground state energy as the free electron model! To describe the metallic bound state one has to respect the antisymmetry of the wave function with respect to interchange of any two particles. Fortunately, in this Hartree-Fock approximation, the plane waves still provide a consistent basis, yet the single particle energies are different from the free-electron energy $\epsilon_{\mathbf{k}}$, Fig 2. As a result, the ground-state energy (per electron) is:

$$E_0/N = \frac{e^2}{8\pi\epsilon_0a_B} \left[\frac{3}{5}(k_F a_B)^2 - \frac{3}{2\pi}(k_F a_B) \right] = \left[\frac{2.21}{r_s^2} - \frac{0.916}{r_s} \right] R_y \quad (5)$$

The second term in (5) is termed “exchange energy” because it results from the exchange of particles in the antisymmetrized wave-function. The difference between the exact ground state energy and the Hartree-Fock result is -by definition - the “correlation

* Electron charge is $-e$, vectors in boldface, operators and tensors in boldface with hat.

$$\begin{aligned}\hbar\mathbf{q} &= \hbar\mathbf{k}_f - \hbar\mathbf{k}_i \\ \hbar\omega &= \epsilon_f - \epsilon_i \\ \hbar\omega &= a\hbar v_F q + \frac{(\hbar q)^2}{2m_0} \\ \alpha &= -1 \dots 1\end{aligned}$$

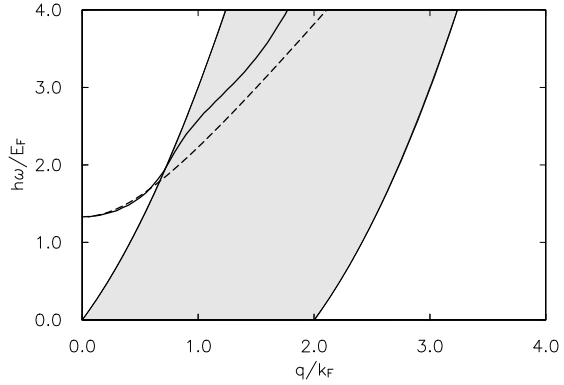


Figure 3. Particle-hole excitation spectrum of a Fermi-gas (dotted area). The solid (dashed) lines display the plasmon-dispersion in a quantum mechanical (hydrodynamic) description. $r_s = 2$.

energy”. For Jellium a bound state is only possible for not too high densities, $r_s > 2.4$. In the low density limit, on the other hand, the electron behavior is dominated by the Coulomb interaction. For $r_s > 100$ the homogeneous state becomes unstable and crystallizes in a “Wigner - lattice”, similar to the ions in a real metal [2,11].

To incorporate influences of the periodic crystal potential and the polarizability of the ions one has to replace the free-electron mass m_0 by a (bandstructure-) effective mass m^* and ϵ_0 by $\epsilon_0\epsilon_\infty$, where the “background” dielectric constant ϵ_∞ accounts for the polarizability of the ion cores. In semimetals and heavily doped degenerate semiconductors the electron densities are quite small compared to ordinary metals, nevertheless their coupling parameter r_s may be even smaller than unity. For the ground state energy of real metals, the energy of the bottom of the band minimum and the electrostatic energy of the ions must be taken into account as well [2].

II. B. Particle - Hole Excitations

Apparently, the simplest type of excitation in a degenerate Fermi-system (at constant particle number) is by pushing one electron out of the Fermi-sea, leaving a hole behind, Fig.2. Conservation of energy and momentum requires $\hbar\mathbf{q} = \hbar\mathbf{k}_f - \hbar\mathbf{k}_i$ $\hbar\omega = \epsilon_f - \epsilon_i$ which leads to a quadratic function between ω and q . As a function of the parameter $a = k_i \cos\theta / k_F = -1 \dots 1$ the allowed region of excitations cover an entire region in the $\omega - q$ plane, Fig. 3.

II. C. Collective Excitations: Plasmons

Plasmons are collective excitations of the many electron system, i.e. all particles move coherently with a common frequency and wave-vector. In the long wave-length limit $\lambda \gg 1/k_F$ this mode can be obtained quite simply. In addition we assume only a single band to contribute (one-component plasma). Consider deviations ρ_1 of the electron charge-distribution from its equilibrium value ρ_0 . Then, the total charge distribution

$$\rho(\mathbf{r}, t) = \rho_+ + \rho_0 + \rho_1(\mathbf{r}, t) \quad (6)$$

will be the source of an electrical field

$$\text{div } \mathbf{E}(\mathbf{r}, t) = \rho_1(\mathbf{r}, t) / \epsilon_0, \quad \text{curl } \mathbf{E}(\mathbf{r}, t) \approx 0. \quad (7)$$

Due to charge neutrality $\rho_0 + \rho_+ = 0$. In addition, the charge- and current density must obey the continuity equation

$$\frac{\partial \rho(\mathbf{r}, t)}{\partial t} + \text{div } \mathbf{j}(\mathbf{r}, t) = 0 \quad (8)$$

where $\mathbf{j}(\mathbf{r}, t) = \rho(\mathbf{r}, t)\mathbf{v}(\mathbf{r}, t)$ and $\mathbf{v}(\mathbf{r}, t)$ denotes the mean velocity of the electrons. Finally, we need an equation to link the electron-velocity to the electrical field. In a hydrodynamic-like description this equation reads (see appendix A1):

$$m_0 n(\mathbf{r}, t) \frac{\partial \mathbf{v}}{\partial t} + \text{grad} P(\mathbf{r}, t) = -en(\mathbf{r}, t)\mathbf{E}(\mathbf{r}, t). \quad (9)$$

For low frequencies local thermodynamic equilibrium would hold and $P(\mathbf{r}, t) = 2E/3V = 2\varepsilon_F n(\mathbf{r}, t)/5$ is the pressure of the electron gas (at constant temperature, $T = 0$). For small amplitude oscillations, $|\rho_1| \ll |\rho_0|$, we obtain

$$\left[\frac{\partial}{\partial t} + \gamma \right] \mathbf{j}(\mathbf{r}, t) = \frac{n_0 e^2}{m_0} \mathbf{E}(\mathbf{r}, t) - \beta \text{grad} \rho_1(\mathbf{r}, t) \quad (10)$$

γ accounts for additional damping processes. Actually, plasma oscillations are a high frequency phenomenon so that the correct value for β is different from $\beta_{hyd} = v_F^2/3$. In the “random phase approximation” which is valid for $r_s < 1$ $\beta_{RPA} = 3v_F^2/5$ [2,4]. Eq. (10) is a generalization of the Drude-theory to inhomogeneous fields.

Assuming wave-like behaviour of all fields, e.g., $\rho_1(\mathbf{r}, t) \propto \exp[i(\mathbf{q}\mathbf{r} - \omega t)]$ and $\mathbf{E}, \mathbf{j} \parallel \mathbf{q}$, we obtain for the plasmon–dispersion

$$\omega_{bp}(q) = \sqrt{\omega_p^2 + \beta q^2} = \omega_p \left[1 + \frac{\beta}{2\omega_p^2} q^2 + \dots \right]. \quad (11)$$

Bulk plasmons are, thus, longitudinally polarized charge–density waves. For neutral Fermi-systems ($\omega_p = 0$) like liquid ${}^3\text{He}$ the collective mode is a low-frequency phenomenon with sound-like dispersion $\omega = c_0 q$, $c_0 = v_F/\sqrt{3}$.

For small wave vectors, the stability of the plasmon is obvious from Fig. 3: the decay into a single electron-hole pair is forbidden by conservation of momentum and energy! Decay into several electron-hole pairs, however, is not excluded, yet as a higher order process it leads only to a small transition rate. For larger wave vectors the plasmon dispersion enters the particle-hole continuum and can decay directly into a single electron-hole pair (Landau-damping). Thus, the plasmon is expected to disappear as a well defined excitation beyond a critical wave-vector $q_c \approx k_F$.

II. D. Interaction with Electromagnetic Fields

It is clearly not feasible to work with the complete microscopic Maxwell-equations for real many particle systems. It is possible, though, to use “macroscopic fields” so that the Maxwell equations still retain their form and to construct reasonable approximations. For an introduction see Wooten [12], whereas, the state of the art of dielectric description of matter is laid down by Kirshnits et al. [13].

In a first step, one decomposes the charge and current densities into “external” and “system” or “induced” quantities.

$$\rho(\mathbf{r}, t) = \rho_{ext}(\mathbf{r}, t) + \rho_{ind}(\mathbf{r}, t), \quad \mathbf{j}(\mathbf{r}, t) = \mathbf{j}_{ext}(\mathbf{r}, t) + \mathbf{j}_{ind}(\mathbf{r}, t). \quad (12)$$

Here the adjective “external” merely refers to the control, not to the location of the sources, i.e. we assume that they are not effected by the fields induced in the system. Instead of $\rho_{ext}, \mathbf{j}_{ext}$ one often uses $\mathbf{E}_{ext}, \mathbf{B}_{ext}$, the external fields in the absence of the system charges.

For time-dependent fields, there is only but one independent “matter field”, $\mathbf{j}_{ind}(\mathbf{r}, t)$, - the charge density is already fixed (up to a constant) by integration of the continuity equation.

$$\frac{\partial \rho_{ind}(\mathbf{r}, t)}{\partial t} + \text{div} \mathbf{j}_{ind}(\mathbf{r}, t) = 0. \quad (13)$$

Instead of $\mathbf{j}_{ind}(\mathbf{r}, t)$ one often introduces two other fields \mathbf{P}, \mathbf{M} , the polarization and magnetization, by requiring

$$\mathbf{j}_{ind}(\mathbf{r}, t) = \frac{\partial \mathbf{P}(\mathbf{r}, t)}{\partial t} + \text{curl} \mathbf{M}(\mathbf{r}, t), \quad \rho_{ind}(\mathbf{r}, t) = -\text{div} \mathbf{P}(\mathbf{r}, t). \quad (14)$$

Equations (14) automatically fulfill the continuity equation for the system charges. Such a decomposition is particularly useful for quasistatic fields for which \mathbf{P}, \mathbf{M} were originally constructed. In addition, one tacitly assumes that $\text{curl} \mathbf{P} = 0$. For high frequencies, however, the decomposition of the current in terms of polarization and magnetization currents is ambiguous and one may put $\mathbf{M} = 0$ without loss of generality! In this “gauge” $\mathbf{D} = \epsilon_0 \mathbf{E} + \mathbf{P}$, $\mathbf{B} = \mu_0 \mathbf{H}$ and the Maxwell equations become particularly simple:

$$\begin{aligned} \text{curl} \mathbf{E}(\mathbf{r}, t) &= \frac{\partial \mathbf{B}(\mathbf{r}, t)}{\partial t}, & \text{curl} \mathbf{B}(\mathbf{r}, t) &= \mu_0 \left(\mathbf{j}_{ext}(\mathbf{r}, t) + \frac{\partial \mathbf{D}(\mathbf{r}, t)}{\partial t} \right), \\ \text{div} \mathbf{D}(\mathbf{r}, t) &= \rho_{ext}(\mathbf{r}, t), & \text{div} \mathbf{B}(\mathbf{r}, t) &= 0. \end{aligned} \quad (15)$$

To specify the system under consideration, the Maxwell-equations must be supplemented by “material” equations, which - like (10) - link \mathbf{j}_s or \mathbf{P}, \mathbf{M} to the external (or total) fields. On a phenomenological level, this can be achieved by

$$\mathbf{D}(\mathbf{r}, t) = \epsilon_0 \hat{\epsilon} \mathbf{E}(\mathbf{r}, t) = \epsilon_0 \int \int \epsilon(\mathbf{r}, \mathbf{r}', t - t') \mathbf{E}(\mathbf{r}', t') d^3 \mathbf{r}' dt' \quad (16)$$

or by the inverse relation

$$\mathbf{E}(\mathbf{r}, t) = \frac{1}{\epsilon_0} \hat{\epsilon}^{-1} \mathbf{D}(\mathbf{r}, t) = \frac{1}{\epsilon_0} \int \int \epsilon^{-1}(\mathbf{r}, \mathbf{r}', t - t') \mathbf{D}(\mathbf{r}', t') d^3 \mathbf{r}' dt' \quad (17)$$

where $\epsilon^{-1}(\mathbf{r}, \mathbf{r}', t - t')$ denotes the kernel of the operator $\hat{\epsilon}^{-1}$ which is inverse to $\hat{\epsilon}$.

For infinite, homogeneous systems, $\epsilon(\mathbf{r}, \mathbf{r}', t - t')$ is solely a function of $\mathbf{r} - \mathbf{r}'$ and the Maxwell-equations can be simplified by Fourier-transformation.

$$\begin{aligned} \mathbf{E}(\mathbf{r}, t) &= \int \int \mathbf{E}(\mathbf{q}, \omega) e^{i(\mathbf{q}\mathbf{r} - \omega t)} \frac{d^3 \mathbf{q} d\omega}{(2\pi)^4}, & \mathbf{D}(\mathbf{q}, \omega) &= \epsilon_0 \epsilon(\mathbf{q}, \omega) \mathbf{E}(\mathbf{q}, \omega), \\ \mathbf{E}(\mathbf{q}, \omega) &= \int \int \mathbf{E}(\mathbf{r}, t) e^{-i(\mathbf{q}\mathbf{r} - \omega t)} d^3 \mathbf{r} dt, & \epsilon(\mathbf{q}, \omega) &= \int \int \epsilon(\mathbf{r}, t) e^{-i(\mathbf{q}\mathbf{r} - \omega t)} d^3 \mathbf{r} dt. \end{aligned} \quad (18)$$

To solve the following set of algebraic equations,

$$\begin{aligned} i \mathbf{q} \times \mathbf{E}(\mathbf{q}, \omega) &= i \omega \mathbf{B}(\mathbf{q}, \omega), & i \mathbf{q} \times \mathbf{B}(\mathbf{q}, \omega) &= \mu_0 (\mathbf{j}_{ext}(\mathbf{q}, \omega) - i \omega \mathbf{D}(\mathbf{q}, \omega)), \\ i \mathbf{q} \cdot \mathbf{D}(\mathbf{q}, \omega) &= \rho_{ext}(\mathbf{q}, \omega), & i \mathbf{q} \cdot \mathbf{B}(\mathbf{q}, \omega) &= 0, \end{aligned} \quad (19)$$

it is convenient to decompose all vector-fields into longitudinal and transverse components with respect to wave vector \mathbf{q} , i.e.

$$\mathbf{E}(\mathbf{q}, \omega) = \mathbf{E}_\ell + \mathbf{E}_t = (\mathbf{E} \cdot \mathbf{n}_\ell) \mathbf{n}_\ell + \mathbf{n}_\ell \times (\mathbf{E} \times \mathbf{n}_\ell) \quad (20)$$

with unit vector $\mathbf{n}_\ell = \mathbf{q} / |\mathbf{q}|$. Even for homogeneous and isotropic systems, like Jellium, the reaction of the charged particles with respect to transverse and longitudinal fields is different, i. e. $\epsilon(\mathbf{q}, \omega)$ is still a tensor with two different principal components $\epsilon_\ell, \epsilon_t$.

$$\mathbf{D}(\mathbf{q}, \omega) = \epsilon_0 \epsilon(\mathbf{q}, \omega) \mathbf{E}(\mathbf{q}, \omega) = \epsilon_0 \epsilon_\ell(\mathbf{q}, \omega) \mathbf{E}_\ell + \epsilon_0 \epsilon_t(\mathbf{q}, \omega) \mathbf{E}_t(\mathbf{q}, \omega) \quad (21)$$

$\epsilon_\ell(0, \omega) = \epsilon_t(0, \omega)$ is the “optical” dielectric function $\epsilon(\omega)$. The solution of (19) is given by

$$\begin{aligned} D_\ell(\mathbf{q}, \omega) &= \frac{-i}{q} \rho_{ext}(\mathbf{q}, \omega), & \mathbf{D}_t(\mathbf{q}, \omega) &= \epsilon_0 \epsilon_t(\mathbf{q}, \omega) \mathbf{E}_t(\mathbf{q}, \omega), \\ E_\ell(\mathbf{q}, \omega) &= \frac{-i \rho_{ext}(\mathbf{q}, \omega)}{\epsilon_0 \epsilon_\ell(\mathbf{q}, \omega) q}, & \mathbf{E}_t(\mathbf{q}, \omega) &= \frac{i \omega \mathbf{j}_{ext}(\mathbf{q}, \omega)}{\epsilon_0 [c^2 q^2 - \omega^2 \epsilon_t(\mathbf{q}, \omega)]}, \\ B_\ell(\mathbf{q}, \omega) &= 0, & \mathbf{B}_t(\mathbf{q}, \omega) &= \frac{1}{\omega} \mathbf{q} \times \mathbf{E}_t(\mathbf{q}, \omega). \end{aligned} \quad (22)$$

The longitudinal component of the external current satisfies $(\mathbf{j}_{ext} - i \omega \mathbf{D})_\ell = 0$ which is equivalent to the continuity equation. Apparently, \mathbf{B} is purely transverse. For non-relativistic particles, retardation effects may be neglected, hence, the electrical field is almost longitudinal. Furthermore, for slab geometries, \mathbf{D} is identical with $\epsilon_0 \mathbf{E}_{ext}$, the electrical field without the system-charges.

In the hydrodynamic description the required dielectric functions are easily obtained from the Fourier-transformed equations (7,8,10)

$$\varepsilon_\ell(\mathbf{q}, \omega) = 1 - \frac{\omega_p^2}{\omega(\omega + i\gamma) - \beta q^2}, \quad \varepsilon_t(\mathbf{q}, \omega) = 1 - \frac{\omega_p^2}{\omega(\omega + i\gamma)}. \quad (23)$$

Parameters γ, β can be used to fit the measured bulk losses and plasmon-dispersion. In the high density limit $r_s < 1$, $\beta_{RPA} = 3v_F^2/5$ which will be used as a reference. $\varepsilon_t(\mathbf{q}, \omega)$ is identical with the standard Drude theory. Due to the singular structure of the denominator for the transverse fields in (22), this approximation will be sufficient in most cases.

The situation is more subtle for the longitudinal dielectric function. Clearly the hydrodynamic $\varepsilon_\ell(\mathbf{q}, \omega)$ does not properly include particle-hole excitations which requires a microscopic theory, i.e. a kinetic or quantum treatment. Explicit analytical results were first obtained by Lindhard (see [2,4] and appendices A2,3), Fig. 4.

Causality requires that the kernel $\varepsilon(\mathbf{r}, \mathbf{r}', t-t') = 0$ if $t' > t$, i.e. the system cannot react before the perturbation is turned-on. This “trivial” property has deep consequences: In Fourier-space, $\varepsilon_t(\mathbf{q}, \omega)$ is an analytic function in the complex ω -half-plane $\Im \omega > 0$ which, in turn, leads to the Kramers-Kronig relations:

$$\Re \varepsilon_t(\mathbf{q}, \omega) - 1 = \frac{1}{\pi} \rlap{-}\int_{-\infty}^{\infty} \Im \varepsilon_t(\mathbf{q}, \omega') \frac{d\omega'}{\omega' - \omega}, \quad \Im \varepsilon_t(\mathbf{q}, \omega) = -\frac{1}{\pi} \rlap{-}\int_{-\infty}^{\infty} \Re \varepsilon_t(\mathbf{q}, \omega') \frac{d\omega'}{\omega' - \omega}. \quad (24)$$

Symbol “P” denotes “principal value integration”, which is a prescription how to evaluate the singular integrals.

The Kramers-Kronig relations (24) are strictly valid for the transverse dielectric function only. Here, \mathbf{D} is the response on the perturbation \mathbf{E} . For longitudinal fields the situation is opposite. ρ_{ext} , or equivalently \mathbf{D} , plays the role of an (arbitrarily prescribable) perturbation rather than \mathbf{E} . Hence, $\varepsilon^{-1}(\mathbf{r}, \mathbf{r}', t-t') = 0$ if $t' > t$ is a causal function, and $\varepsilon_\ell^{-1}(\mathbf{q}, \omega)$ is analytic in $\Im \omega > 0$ and, correspondingly, the Kramers-Kronig relations read:

$$\Re \frac{1}{\varepsilon_\ell(\mathbf{q}, \omega)} - 1 = \frac{1}{\pi} \rlap{-}\int_{-\infty}^{\infty} \Im \frac{1}{\varepsilon_\ell(\mathbf{q}, \omega')} \frac{d\omega'}{\omega' - \omega}, \quad \Im \frac{1}{\varepsilon_\ell(\mathbf{q}, \omega)} = -\frac{1}{\pi} \rlap{-}\int_{-\infty}^{\infty} \Re \frac{1}{\varepsilon_\ell(\mathbf{q}, \omega')} \frac{d\omega'}{\omega' - \omega}. \quad (25)$$

But, why is $\varepsilon_\ell(\mathbf{q}, \omega)$ not “as good” as $\varepsilon_\ell^{-1}(\mathbf{q}, \omega)$? $\varepsilon_\ell^{-1}(\mathbf{q}, \omega)$ may well have a zero in $\Im \omega > 0$ so that its inverse would have a pole at just this frequency. Obviously, $\varepsilon_\ell(\mathbf{q}, \omega)$ wouldn’t be analytic in $\Im \omega > 0$ which, by “backshooting” kills causality between the longitudinal \mathbf{D} -response and \mathbf{E} -perturbation. Eq. (24) is correct for transverse fields whereas (25) holds for longitudinal fields! In mathematical terms: The operator $\hat{\varepsilon}$ has a zero eigenvalue (with “transverse eigenfunction”) so that its inverse does not exist. Likewise for $\hat{\varepsilon}^{-1}$ and longitudinal fields. To describe the longitudinal response it is best to introduce a (longitudinal) susceptibility $\chi(\mathbf{q}, \omega)$ as it is done in microscopic treatments

$$\frac{1}{\varepsilon_\ell(\mathbf{q}, \omega)} = 1 + \frac{e^2}{\epsilon_0 q^2} \chi(\mathbf{q}, \omega) = \frac{\rho(\mathbf{q}, \omega)}{\rho_{ext}(\mathbf{q}, \omega)} = \frac{\Phi(\mathbf{q}, \omega)}{\Phi_{ext}(\mathbf{q}, \omega)}. \quad (26)$$

$\chi(\mathbf{q}, \omega)$ denotes the Fourier-transform of the density response function [2,4,12,13]

$$\chi(\mathbf{r}, \mathbf{r}', t-t') = -\frac{i}{\hbar} \theta(t-t') \langle\langle [\hat{N}(\mathbf{r}, t), \hat{N}(\mathbf{r}', t')] \rangle\rangle \quad (27)$$

which is related to the dynamic form factor $S(\mathbf{q}, \omega)$ by

$$\begin{aligned} \chi(\mathbf{q}, \omega) &= \int_0^\infty S(\mathbf{q}, \omega') \left[\frac{1}{\hbar(\omega - \omega') + i\delta} - \frac{1}{\hbar(\omega + \omega') + i\delta} \right] d\omega', \\ S(\mathbf{q}, \omega) &= \frac{1}{\Omega} \sum_m |\langle m | \hat{N}_\mathbf{q}^\dagger | 0 \rangle|^2 \delta(\hbar\omega - E_m + E_0), \quad \omega > 0. \end{aligned} \quad (28)$$

$|m\rangle$, E_m are the exact many-body states and energies, Ω is the volume, and $\hat{N}(\mathbf{r}, t)$ is the density operator. Clearly, the poles of $\chi(\mathbf{q}, \omega)$ are identical with the excitation energies of the many body system.

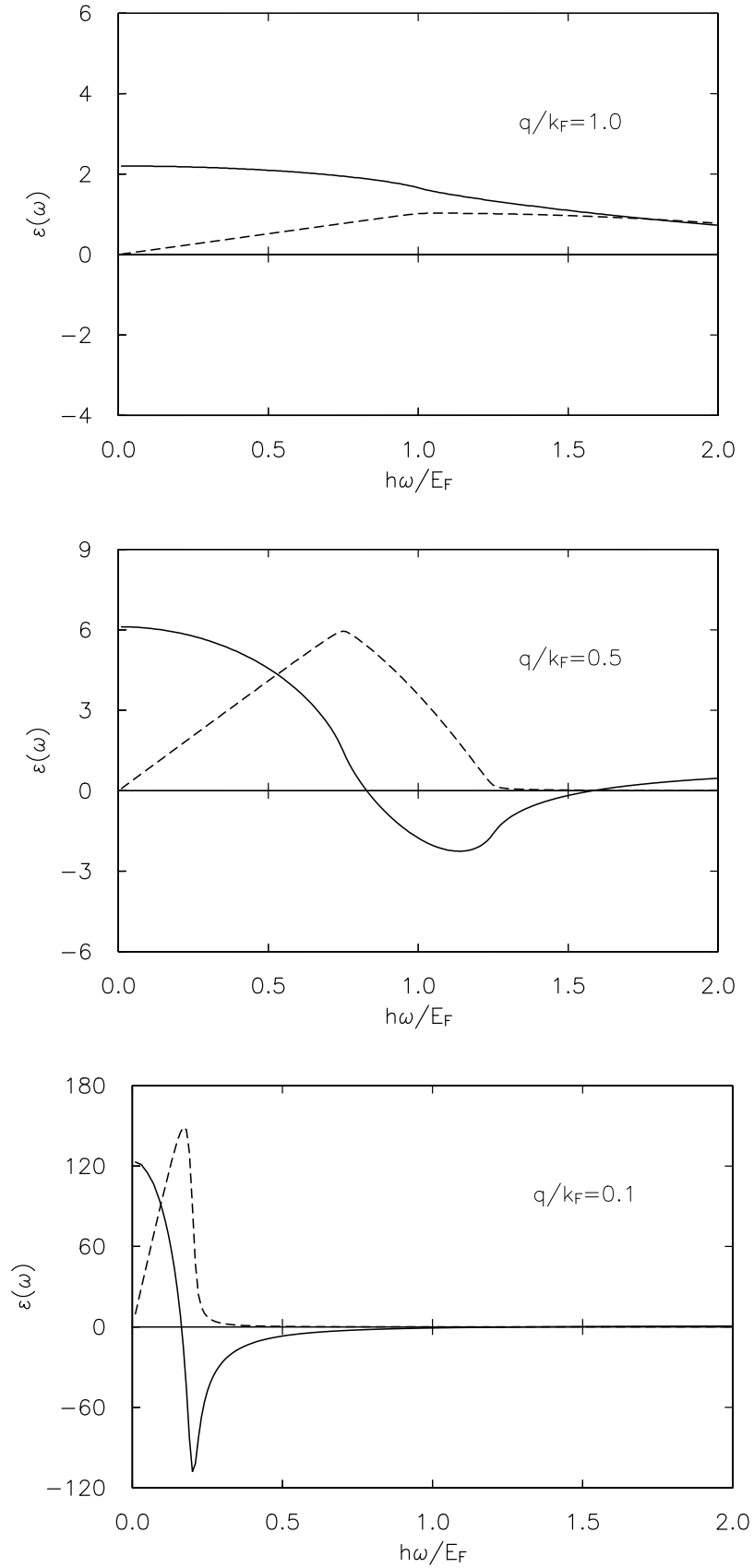


Figure 4. Real part (solid lines) and imaginary part (dotted lines) of the Lindhard dielectric function. $r_s = 2$.

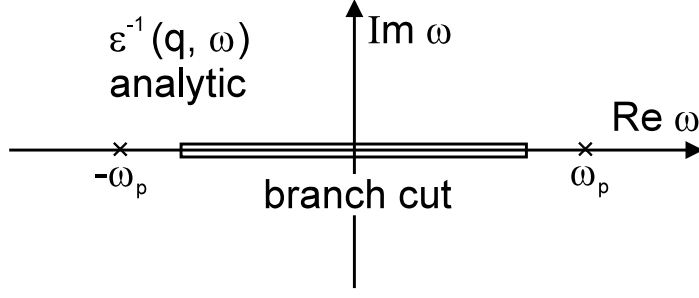


Figure 5. Location of singularities of $\chi(\mathbf{q}, \omega)$ in RPA. The branch cut describes the particle-hole excitations whereas the poles correspond to the plasmon-mode.

With the aid of (24,25) and the high frequency behaviour of $\varepsilon(\mathbf{q}, \omega) \rightarrow 1 - (\omega_p/\omega)^2$ one can prove the following sum rules[2,4]

$$\int_0^\infty \omega \Im \frac{-1}{\varepsilon_\ell(\mathbf{q}, \omega)} d\omega = \int_0^\infty \omega \Im \varepsilon_t(\mathbf{q}, \omega) d\omega = \frac{\pi}{2} \omega_p^2. \quad (29)$$

Due to the translational symmetry of Jellium, the $q = 0$ limit of the exact dielectric function is identical with the Drude-result in the absence of scattering

$$\varepsilon_\ell(0, \omega) = \varepsilon_t(0, \omega) = 1 - \frac{\omega_p^2}{\omega^2}. \quad (30)$$

III. BULK PLASMONS

III. A. Dispersion, Life-Time, and Oscillator Strength

A collective excitation always corresponds to a possible oscillation of the system in the absence of an external field. Apparently, the dispersion relation $\omega_{bp}(q)$ of these modes is given by the poles of the density response function $\chi(\mathbf{q}, \omega)$, or equivalently, the zeros of $\varepsilon_\ell(\mathbf{q}, \omega)$:

$$\chi(\mathbf{q}, \omega) = \infty, \quad \text{or} : \varepsilon_\ell(\mathbf{q}, \omega) = 0. \quad (31)$$

Bulk plasmons are purely electrical waves, $\mathbf{B} = 0$.

Causality warrants that the solutions of (31) are located on the real ω -axis or in the lower ω -half-plane when continuing $\chi(\mathbf{q}, \omega)$ analytically to $\Im \omega < 0$.

$$\omega = \omega_b(q) - i\Gamma(q), \quad \Gamma(q) = \hbar/\tau > 0. \quad (32)$$

where τ is the plasmon life-time. Well defined collective modes are only those solutions with $\Gamma \ll \omega_p$, Fig. 5.

The solutions of (31) lead to peaks in the loss-function

$$P_0(\mathbf{q}, \omega) = \Im \frac{-1}{\varepsilon_\ell(\mathbf{q}, \omega)} \quad (33)$$

which describes the power dissipated by the external field, Fig. 6. Branch-cuts corresponding to the particle-hole excitation continuum may lead to peaks in the loss-function which will be hard to distinguish experimentally from “true” collective modes.

In the small- q limit the dispersion is parabolic and their line-width is zero for $q < q_c \approx \omega_p/v_F$ within the kinetic or RPA theory. If the pole is close to the real ω -axis we may write

$$P_0(\mathbf{q}, \omega) = \frac{\Re Z(q) \Gamma(q) - \Im Z(q) [\omega - \omega_{bp}(q)]}{[\omega - \omega_{bp}(q)]^2 + \Gamma^2(q)} + P_{inc}(\mathbf{q}, \omega), \quad (34)$$

$$Z^{-1}(q) = \frac{\partial \varepsilon(\mathbf{q}, \omega)}{\partial \omega}, \quad \omega = \omega_{bp}(q),$$

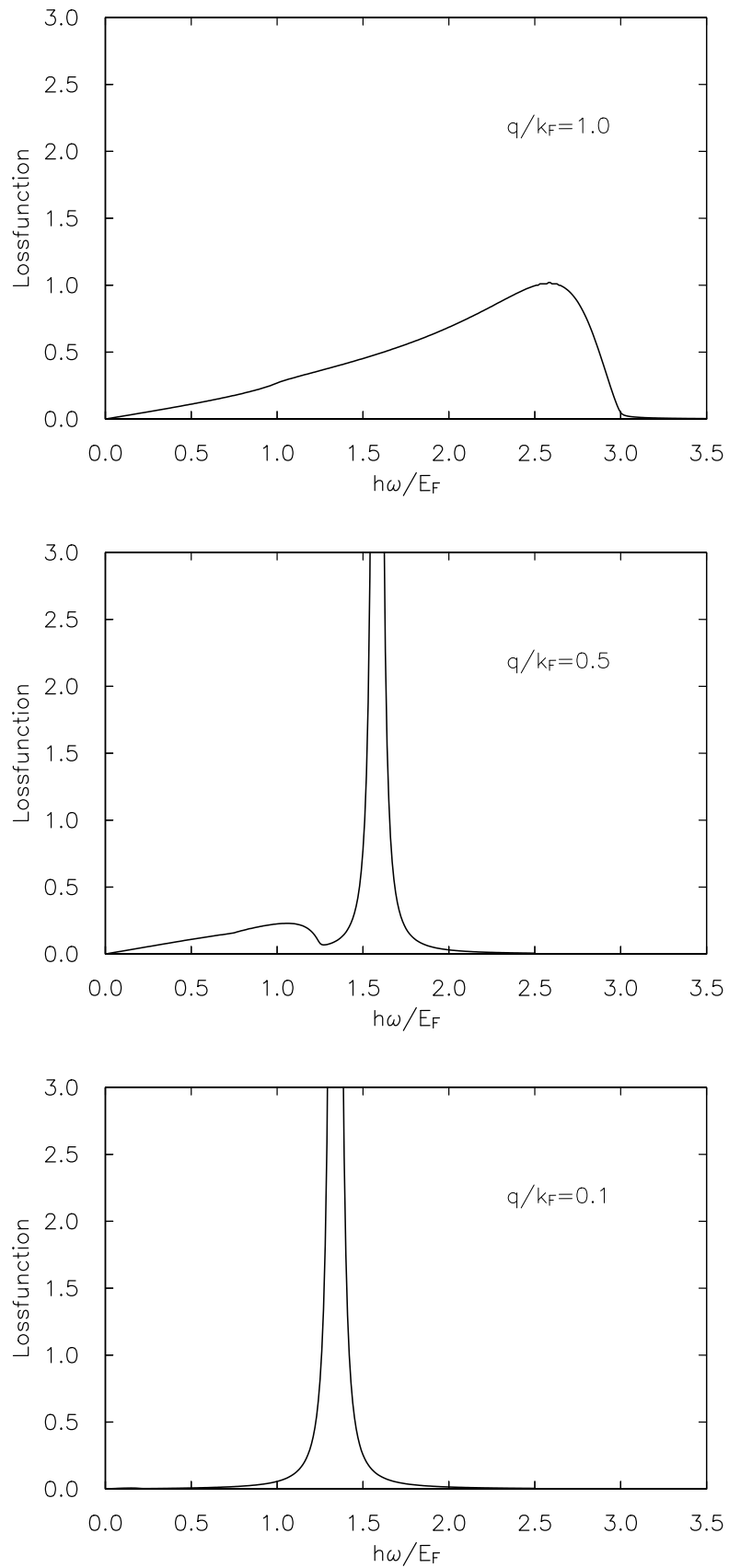


Figure 6. Loss-function for the Lindhard dielectric function [A3]. Instrumental resolution is simulated giving ω a small imaginary part of $0.01E_F$. $r_s = 2$.

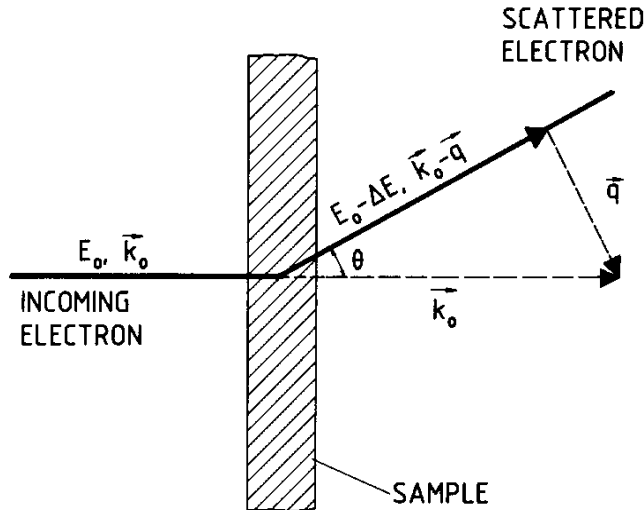


Figure 7. Geometry of the electron–energy–loss scattering experiment [9]

where $Z(q)$ is the residue of the pole which is the plasmon-oscillator strength. $P_{inc}(\mathbf{q}, \omega)$ describes the “incoherent” background contribution of the particle-hole excitation continuum. If $\Im Z(q) \ll \Re Z(q)$ the plasmon line-shape is lorentzian with width $\Gamma(q)$. Due to the sum-rule (29), $Z(q)$ is largest at $q = 0$, and decreases with increasing momentum transfer. Thus the plasmon is the dominant feature in $P(\mathbf{q}, \omega)$ at low momentum transfer.

III. B. Fundamentals of Electron-Energy-Loss-Spectroscopy (EELS)

Spectroscopy of plasmons requires the interaction with electromagnetic fields, either by radiation or with charged particles like fast electrons. As plasmons are longitudinal polarized they don’t couple directly to transverse electromagnetic waves. An almost ideal tool, are fast (but nonrelativistic) electrons, which interact quasistatically via their Coulomb-field “flying” with them [2,5-9]. We follow Fink [9] on “recent developments on electron-energy-loss-spectroscopy”.

The geometry of an EELS experiment is shown in Fig. 7. In the Karlsruhe-spectrometer of Dr. Fink (now at IFW Dresden) the primary energy is $E_0 = 170\text{keV}$ which corresponds to $k_0 = 228.4\text{\AA}^{-1}$. The scattered electrons are analyzed with respect to energy- and momentum transfer. Small q ’s require very small scattering angles, i.e. for $q = 1\text{\AA}^{-1}$ the scattering angle is $4\text{mrad} \approx 0.25^\circ$. Decomposition of the scattering wave vector into components parallel and perpendicular to the incoming beam reveals

$$q_{\parallel} \approx k_0(\hbar\omega/2E_0), \quad q_{\perp} \approx k_0 \sin \theta, \quad (35)$$

with $q^2 = q_{\parallel}^2 + q_{\perp}^2$. Optimum resolution of the instrument is achieved at lowest beam current (15nA , beam cross section is 0.5mm after passing the monochromator): $\Delta E = 80\text{meV}$, $\Delta q = 0.04\text{\AA}^{-1}$ (full width at half maximum).

The basic quantity measured is the differential cross-section which, as usual, can be factorized in an atomic form factor (=Rutherford cross section) and in the structure function $S(\mathbf{q}, \omega)$ which contains the dynamics of the system [2,5]. Instead of $S(\mathbf{q}, \omega)$ EELS–spectroscopists prefer the loss function $P_0(\mathbf{q}, \omega)$.

$$\frac{d^2\sigma}{d\Omega d(\hbar\omega)} = \frac{4}{a_B^2 q^4} S(\mathbf{q}, \omega) = \frac{\hbar}{(\pi a_B)^2} \frac{1}{q^2} P_0(\mathbf{q}, \omega). \quad (36)$$

The EELS cross-section decreases with increasing momentum transfer. For X-ray scattering the situation is opposite, yet EELS-resolution is much better.

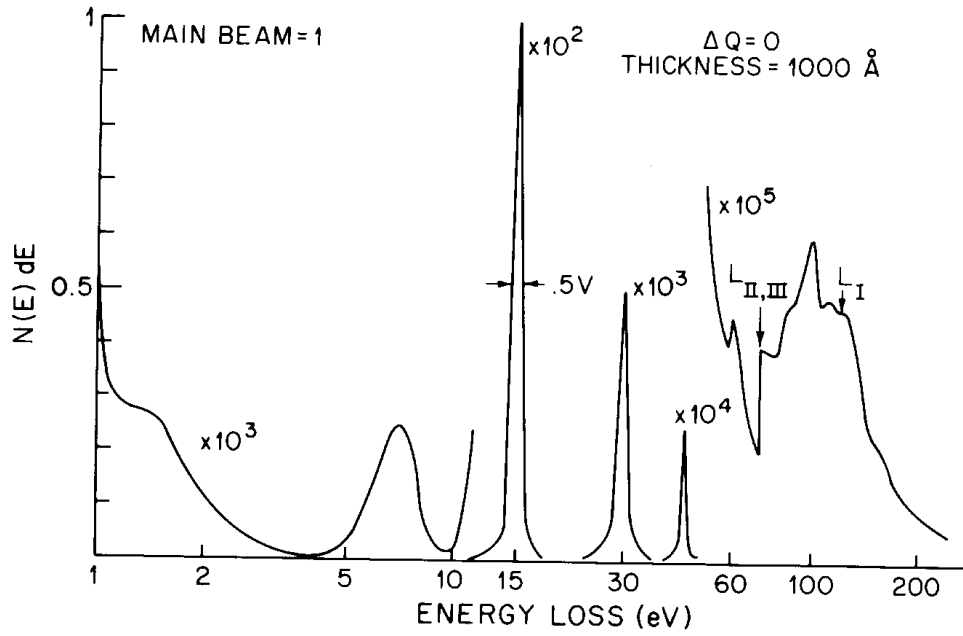


Fig.8. Excitation spectrum of Al in the range 1-250 eV. From Schnatterly [8].

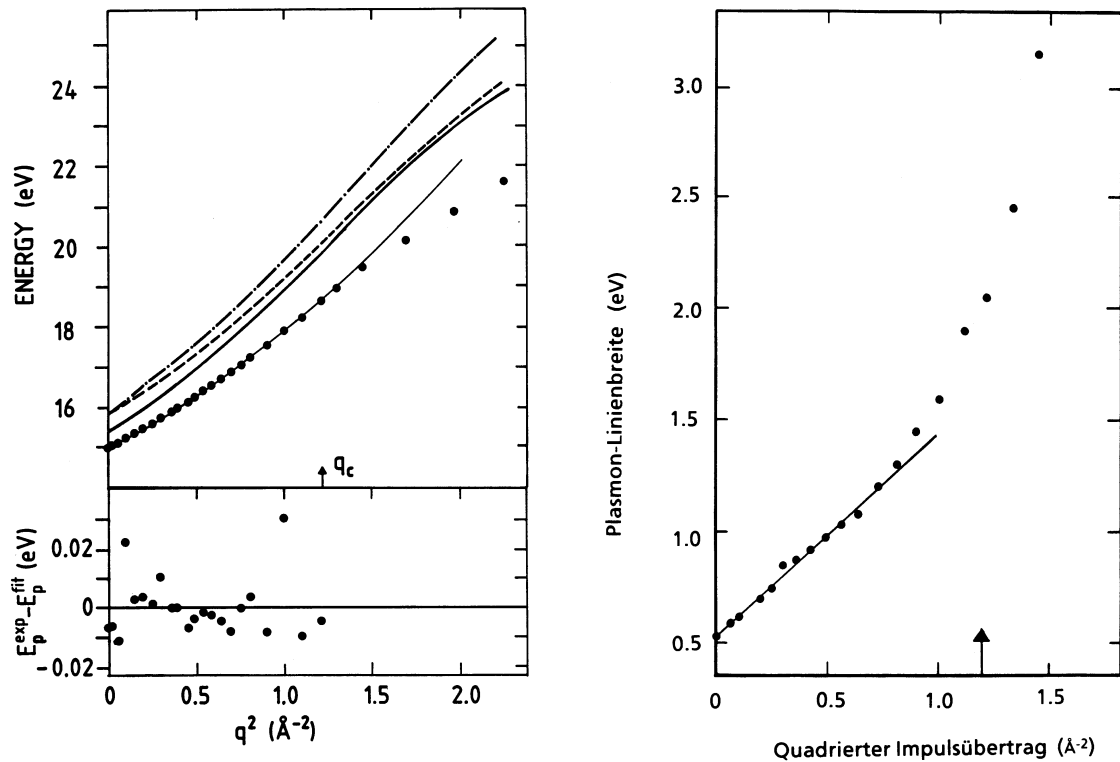


Figure 9. Measured plasmon-dispersion and line-width in Al parallel to [100] direction compared to least square fit curve (thin line) and theories. From Sprösser-Prou et al. [14].

III. C. Experimental Results

In the last two decades plenty of experimental and theoretical work has been performed on the dispersion of plasmons as well as on other excitations in metals. In particular, the simple metals like *Al* and the alkali metals (apart from *Li*) are regarded as nature's closest realization of Jellium. In these metals, band structure effects are expected to be small so that exchange and correlation effects may be studied. For a survey on other materials see Raether [7].

Fig. 8 shows, as an example, the measured excitation spectrum of *Al*. In order of increasing energy the features of the spectrum are: an interband transition at 1.5eV, the surface plasmon at 7eV (oxidized surface), the bulk plasmon at 15eV, multiple excitation of plasmons, and the $L_{II,III}$ soft X-ray threshold at 72.5eV etc. With one instrument, all the elementary excitations from the near IR to the soft X-ray region can be studied [8].

Results of a high resolution ELS study of the bulk plasmon dispersion with respect to the absolute value and orientation of the transferred momentum in an *Al* single crystal are shown in Fig.9. The dispersion has been observed to be biquadratic in q with unique parameters over the entire q range up to the cut-off wave-vector, in contrast to earlier studies as summarized e.g. in [7].

$$\hbar\omega_{bp}(q) = \hbar\omega_p + \alpha \frac{(\hbar q)^2}{m_0} + Bq^4. \quad (37)$$

However, substantial deviations from the *RPA* result $\alpha_{RPA} = \frac{3}{5}\epsilon_F/\hbar\omega_p = 0.44$ have been found: $\alpha_{exp} = 0.30$. Beyond the cut-off q_c (indicated by an arrow) the plasmon still exists but with an increased line-width.

Plasmon dispersion in the alkali's seems to be even more puzzling, Fig. 10. Previous measurements of plasmon-dispersion in simple metals always showed a positive, quadratic dispersion. *Rb* is the first metal with almost no dispersion at all. The deviations become even more pronounced in the case of *Cs* which exhibits a negative dispersion. Deviations do not only occur with respect to the *RPA*, but to improved theories as well, Fig. 11. Particularly, the deviations increase with r_s and indicate the increasing influence of correlation effects in the metallic regime. One might interpret the negative dispersion in *Cs* as an incipient Wigner-crystallization of the electrons.

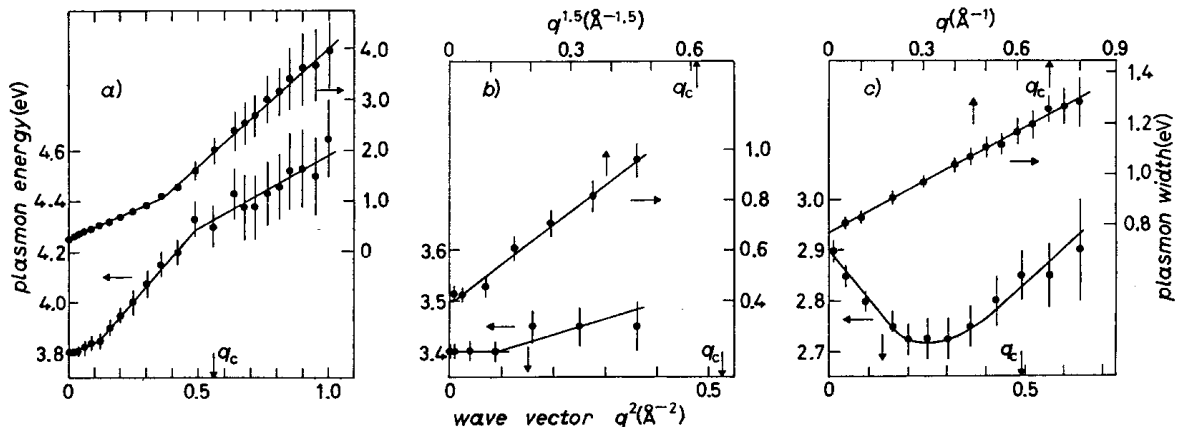


Figure 10. Plasmon dispersion for polycrystalline *K*, *Rb*, and *Cs* (a-c). From v. Felde et al. [15].

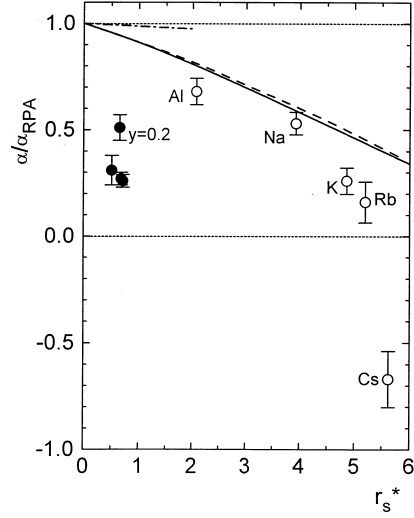


Figure 11. Normalized plasmon dispersion coefficient as a function of the density parameter r_s . Dotted line: RPA, solid and dashed lines: theory by Vashishta and Singwi [16] and Dabrowski [17]. From v. Felde et al. [15].

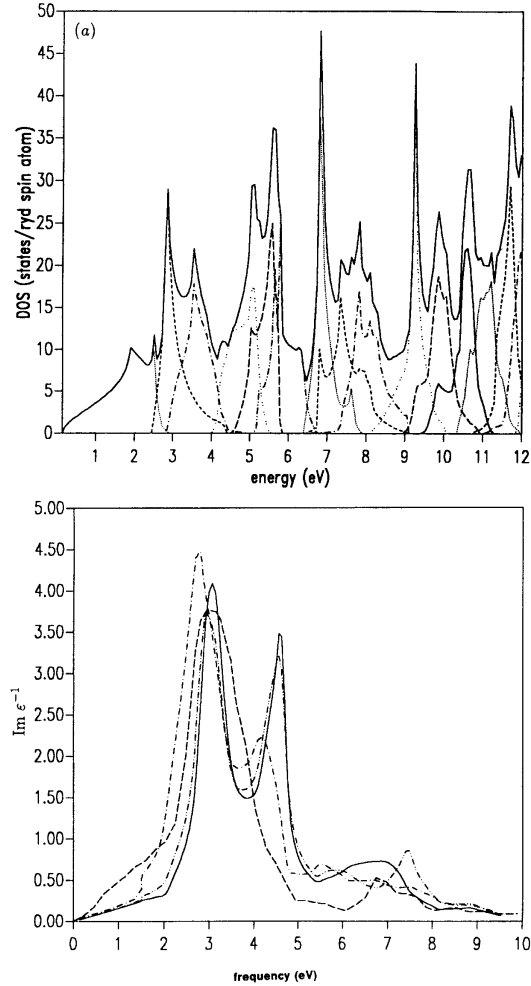


Figure 12. Calculated excitation spectrum of Cs. Upper part: Total density of states (solid line) and contributions from individual bands (broken lines). Fermi energy is 1.88eV . Lower part: Loss function for some wave vectors along the $(1, 0, 0)$ direction. $\mathbf{q} = 2\pi\kappa(1, 0, 0)/a$, for $\kappa = 0.1, 0.2, 0.3, 0.6$ (full, dashed-double dotted, dashed-dotted, and dashed lines). From Kollwitz and Winter [20].

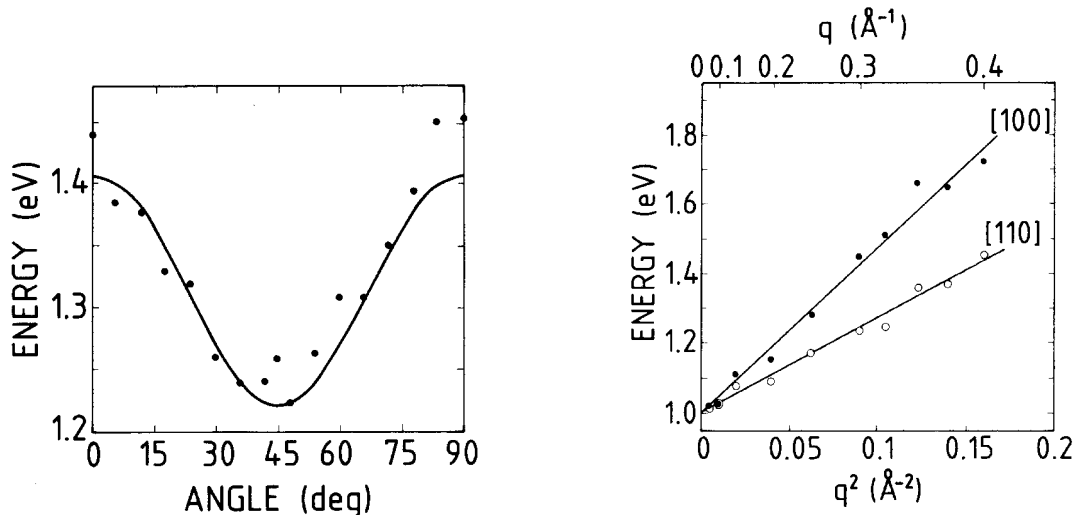


Figure 13. Angle dependence (left) and dispersion (right) of the bulk-plasmon in $Bi_2Sr_2CaCu_2O_8$, a high T_c superconductor in the normal state. From Nücker et al. [22].

The construction of a reasonable approximation for the interacting electron gas in the intermediate coupling range is a long standing problem. Deviations from the *RPA* arise from the neglected exchange and correlation as well as from the periodic crystal potential, which, both reduce α with respect to the *RPA* result. Up to 1986 the theoretical results, e.g. [16-17] converged to the result displayed in Fig. 11 by the solid and dashed lines. Remarkably, the results of these ambitious many-body theories agrees very well with a kinetic theory when the many-body interactions are included by a standard density functional description, appendix A2, where

$$\alpha/\alpha_{RPA} = 1 - \left[0.092r_s + \frac{0.0034r_s^2}{1 + r_s/21} \right]. \quad (38)$$

Stimulated by the experimental results by v. Felde et al. [15] several groups obtained a qualitative improvement. Taut and Sturm [18] considered the combined effect of exchange-correlation and crystal potential and Lipparini et al. [19] worked out a sum-rule approach taking multipair excitations into account. Kollwitz and Winter [20] and Aryasetiawan and Karlson [21] calculated the density response function within a *LDA* formalism. The *Cs*-density of states resembles those of a transition metal, Fig 12. Thus, the heavier alkalis are not free-electron-like metals!

Fig. 13 gives the “in-plane” plasmon dispersion at 300K in $Bi_2Sr_2CaCu_2O_8$ - one of the new high T_c superconductors [22]. The most important bands are essentially formed by the occupied orbitals in the *Cu* - *O* plane. Those with the largest overlap being the *Cu* $3d_{x^2-y^2}$ and the *O* $2p_x$, *O* $2p_y$ orbitals forming a quasi two-dimensional tight-binding bandstructure

$$E(\mathbf{k}) = -\frac{1}{2}t \left[\cos(k_x a) + \cos(k_y a) \right] \quad (39)$$

with $t \approx 1.5eV$ and *O* - *O* distance $a = 3.8\text{\AA}$. Approximating the matrix elements in the *RPA* dielectric function, A3, by their free electron values (=1)

$$\varepsilon(\mathbf{q}, \omega) = 1 - \frac{e^2}{\epsilon_0 q^2} 4 \int \frac{d^3 \mathbf{k}}{(2\pi)^3} f(E(\mathbf{k})) \frac{\Delta E}{(\hbar\omega + i0)^2 - (\Delta E)^2} \quad (40)$$

where $\Delta E = E(\mathbf{k} + \mathbf{q}) - E(\mathbf{k})$ the plasmon dispersion becomes in the $q \rightarrow 0$ limit [22]

$$\hbar\omega_{bp}(\mathbf{q}) = \sqrt{(\hbar\omega_p)^2 + \frac{1}{6}(ta)^2 q^2 \left[\frac{3}{2} + \frac{1}{2} \cos 4\phi \right]}, \quad (41)$$

where ϕ is the angle between \mathbf{q} in the *x* - *y* plane and the *x* axes. Other parameters are $\epsilon_\infty = 4.5$, $m^*/m_0 = 1.7$, $n_0 = 9 \times 10^{21} cm^{-3}$. There is a remarkable good agreement with experiment.

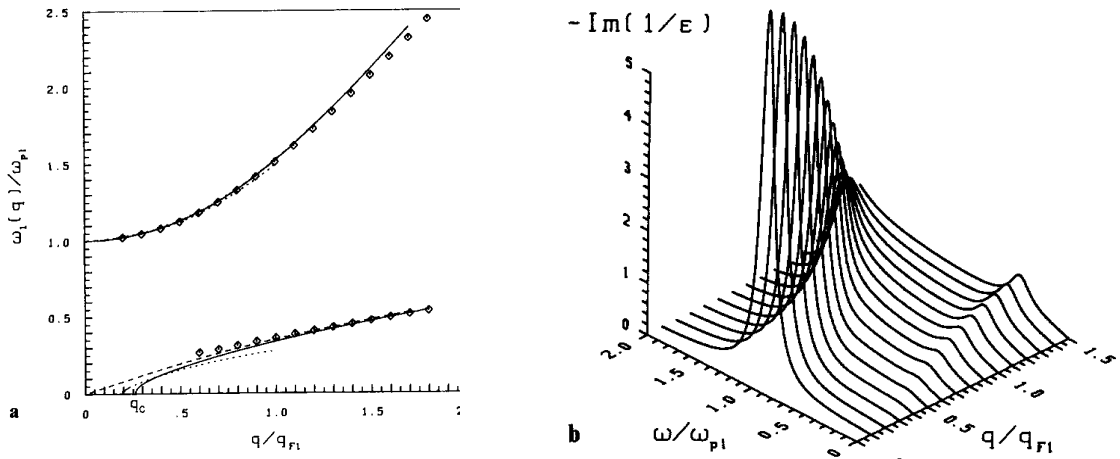


Figure 14. Dispersion (left) and Loss-function (right) of a two component Fermi-system. $\omega_{p2} = 0.5\omega_{p1}$, $\tau_1 = \tau_2 = 71/\omega_{p1}$. Dashed lines: $\tau_j = \infty$. From [27].

III. D. Acoustic Plasmons in a Two-Component Fermi-System

A Fermi-system with two (or more) different types of mobile charge carries e.g. a transition metal with s and d electrons exhibits two distinct collective charge density excitations: a high frequency “optical” plasmon and a sound-like “acoustic” plasmon. The dispersion of these modes, in the limit $q \rightarrow 0$ and in absence of scattering, is given by [23,24],

$$\begin{aligned}\omega_{opt}(q) &= \sqrt{\omega_{p1}^2 + \omega_{p2}^2 + O(q^2)}, \\ \omega_{ac}(q) &= \sqrt{\frac{\omega_{p1}^2\beta_2 + \omega_{p2}^2\beta_1}{\omega_{p1}^2 + \omega_{p2}^2}} q.\end{aligned}\quad (42)$$

ω_{pj} and β_j denote the plasma frequencies and dispersion coefficients of the components $j = 1, 2$.

In contrast to optical plasmons, which are well-established experimentally, their acoustic counterparts have not yet been unambiguously identified, e.g. [25]. Nevertheless, there are several speculations in serious journals about their relationship to the “old high T_c ” superconductors, e.g. Nb_3Sn [26].

Analogous to plasmons in a one-component Fermi-system the dispersion of acoustic and optical plasmons is obtained from

$$\varepsilon(\mathbf{q}, \omega) = 1 + \Pi_1(\mathbf{q}, \omega) + \Pi_2(\mathbf{q}, \omega) = 0, \quad (43)$$

where $\Pi_j(\mathbf{q}, \omega)$ denotes the polarization of the individual components. In the hydrodynamic description (23), we obtain

$$\varepsilon(\mathbf{q}, \omega) = 1 - \frac{\omega_{p1}^2}{\omega(\omega + i\gamma_1) - \beta_1 q^2} - \frac{\omega_{p2}^2}{\omega(\omega + i\gamma_2) - \beta_2 q^2}. \quad (44)$$

For $\gamma_j = 0$ the two branches of the solutions of (43) are given by (41). Results of a numerical study within a kinetic theory are displayed in Fig. 14. Notice that the acoustic mode is overdamped near $q = 0$ and its oscillator strength is very small.

IV. SURFACE PLASMONS

IV. A. Concept of a Surface Plasmon

The concept of surface plasmons was introduced by Ritchie[28] shortly after the discovery of bulk plasmons in metals. In recent years surface plasmons have been observed in a wide range of materials using both electron and photon spectroscopy. In addition, significant progress has been made towards a systematic use of surface plasmons as a diagnostic tool to investigate the surface charge profile of metals. For surveys see, e.g. Raether [29].

Suppose an electron gas confined to the half-space $z < 0$ with a smooth electron charge distribution near the metal-vacuum boundary, Fig. 15. If an external field acts on the plasma boundary it will induce a charge which is concentrated near the surface,

$$\rho(\mathbf{r}, t) = \Re \left[\exp[i(q_x x - \omega_s t)] d(z) \right], \quad (45)$$

where q_x is the wave number and ω_{sp} the frequency of the surface charge density wave.

For metals, the “spill-off” of the charge density across the geometrical boundary $z = 0$ is of the order of $1/k_F \approx 1\text{\AA}$, so that a macroscopic description may be sufficient for a qualitative understanding of surface charge density wave.

The charge oscillations are in turn the sources of electromagnetic fields. In particular, we are looking for “evanescent” waves, i.e. fields which decay exponentially from the surface. First, $\text{div } \mathbf{E}$ demands:

$$\mathbf{E}(\mathbf{r}, t) = \Re \left[(\alpha A, 0, i q_x A) e^{i(q_x x - \omega t)} e^{-\alpha z} \right] \quad (46)$$

where q_x is the same in both half-spaces but the amplitudes A_{\pm} and decay-constants $\alpha = \pm \alpha_{\pm}$ are different. Second, the wave equation requires

$$\Delta \mathbf{E} + \left(\frac{\omega}{c}\right)^2 \epsilon_{\pm}(\omega) \mathbf{E} = 0, \quad q_x^2 - \alpha_{\pm}^2 = \left(\frac{\omega}{c}\right)^2 \epsilon_{\pm}(\omega), \quad (47)$$

and, third, we have to respect the boundary condition at $z = 0$:

$$\begin{aligned} \text{Continuity of } \mathbf{E}_x: & \quad -\alpha_+ A_+ = \alpha_- A_-, \\ \text{Continuity of } \mathbf{D}_z: & \quad q_x \epsilon_+ A_+ = q_x \epsilon_- A_-. \end{aligned} \quad (48)$$

Nontrivial solutions for A_{\pm} of (48) require the determinant to vanish

$$\alpha_+ \epsilon_-(\omega) + \alpha_- \epsilon_+(\omega) = 0, \quad (49)$$

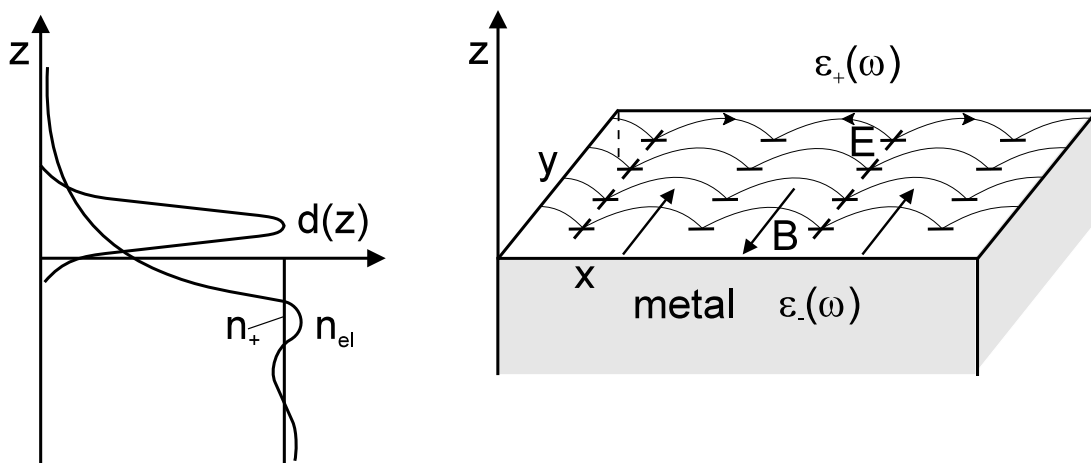


Figure 15. Electron charge distribution (left) and electromagnetic field (right) for a plasmon at a plane surface.

or, when using the relation between α_{\pm} and q_x :

$$\sqrt{q_x^2 - \left(\frac{\omega}{c}\right)^2 \epsilon_+(\omega)} \epsilon_-(\omega) + \sqrt{q_x^2 - \left(\frac{\omega}{c}\right)^2 \epsilon_-(\omega)} \epsilon_+(\omega) = 0. \quad (50)$$

This equation may be solved for q_x as a function of ω

$$q_x^2 = \left(\frac{\omega}{c}\right)^2 \frac{\epsilon_+(\omega)\epsilon_-(\omega)}{\epsilon_+(\omega) + \epsilon_-(\omega)}, \quad (51)$$

which is a true solution only if $\Re \epsilon_+/\epsilon_- < 0$.

For a Drude-metal bounded by a nondispersive dielectric ϵ_b , we have:

$$\omega_{sp}(q_x) = \begin{cases} \frac{c}{\sqrt{\epsilon_b}} q_x \left[1 - \frac{1}{2} \left(\frac{c}{\omega_p}\right)^2 q_x^2 \dots \right], & q_x \ll \omega_p/c \\ \frac{\omega_p}{\sqrt{1 + \epsilon_b}} \left[1 - \frac{1}{2} \left(\frac{\omega_p}{c}\right)^2 \left(\frac{\epsilon_b}{1 + \epsilon_b}\right)^2 q_x^2 \dots \right], & q_x \gg \omega_p/c. \end{cases} \quad (52)$$

Core-polarization effects in the metal can be taken into account by rescaling $\omega_p \rightarrow \omega_p/\sqrt{\epsilon_{\infty}}$, $c \rightarrow c/\sqrt{\epsilon_{\infty}}$, $\epsilon_b \rightarrow \epsilon_b/\epsilon_{\infty}$.

The phase velocity of the surface-plasmon is always smaller than the speed of light in the adjacent dielectric. Thus, without participation of another system which may take-off momentum the surface-plasmon cannot decay radiatively. Even the decay into other surface-plasmons of smaller energy is not possible. Any structural feature which breaks the symmetry of the plane surface, however, may give rise to coupling: surface roughness, phonons, grating-rulings,... (For the discussion of ‘‘radiative plasmons’’ see Raether [29].)

The discussion of surface-plasmons can be alternatively presented as a problem of optics: Does the (inverse) reflection problem have an outgoing solution for vanishing amplitude of the incoming field? [30,31] For p-polarized light the standard Fresnel formulae for the reflection of light at a plane surface are [32]:

$$R_p = \frac{\tan(\alpha - \beta)}{\tan(\alpha + \beta)}, \quad \frac{\sin(\alpha)}{\sin(\beta)} = n_r = \sqrt{\frac{\epsilon_-(\omega)}{\epsilon_+(\omega)}}. \quad (53)$$

R_p denotes the amplitude reflection-coefficient and α, β are related by Snell’s diffraction law which is a consequence of the continuity of q_x at the boundary. (Formally, these relations are valid for complex α and β , too.) In the limit of vanishing incoming amplitude a nonzero outgoing wave is only possible for $R_p = \infty$, i.e. $\alpha - \beta = \pi/2$ or $\cos \alpha = -\sin \beta$. Using $\tan \alpha = q_x/q_{\perp} = -n_r$ and $q_{\perp}^2 + q_x^2 = (\omega/c)^2 \epsilon_+$ immediately leads to (51). ($\alpha = \pi/2 - i\alpha'$). In addition, we notice that $R_p = 0$, i.e. $\alpha + \beta = \pi/2$ is just the condition for the Brewster-angle.

Standard optics for metals as well as for semiconductors is based on the assumption that only transverse electromagnetic waves can propagate in the material. At frequencies comparable with the plasma-frequency the inertia of the conduction electrons prevents instant screening and, besides the transverse electromagnetic waves, a longitudinal plasma wave can propagate inside the metal [31].

An elegant formulation of the reflection properties is by using the surface impedance Z_p (in units of $\sqrt{\mu_0/\epsilon_0} \approx 377\Omega$) [32].

$$R_p(\alpha, \omega) = \frac{Z_p - \cos \alpha}{Z_p + \cos \alpha} \quad (54).$$

For p-polarized light, incident from the vacuum at an angle α from the surface normal, the surface impedance is given by [33]

$$Z_p = \frac{E_x(-0)}{H_y(-0)} = \frac{1}{2\pi} \left(\frac{2i\omega}{c}\right) \int_{-\infty}^{\infty} \frac{dq_z}{q^2} \left[\frac{q_x^2}{(\omega/c)^2 \epsilon_t(q, \omega)} + \frac{q_z^2}{(\omega/c)^2 \epsilon_t(q, \omega) - q^2} \right] \quad (55)$$

where $q^2 = q_x^2 + q_z^2$, $q_x = \omega \sin \alpha/c$. Eq. (55) is valid for a sharp surface and if the electrons are scattered specularly at the surface.

The surface plasmon dispersion is obtained from the pole of (54)

$$\sqrt{q_x^2 - \left(\frac{\omega}{c}\right)^2} = -\frac{2}{\pi} \int_0^\infty \frac{dq_z}{q^2} \left[\frac{q_x^2}{\varepsilon_\ell(q, \omega)} + \frac{q_z^2}{\varepsilon_t(q, \omega) - (cq/\omega)^2} \right]. \quad (56)$$

Result (56) includes many previous results for the sharp-barrier approximation. For example, in the local approximation $\varepsilon_\ell(\mathbf{q}, \omega) = \varepsilon_t(\mathbf{q}, \omega) = \varepsilon(\omega)$ (51) is obtained. If retardation is neglected by letting $c \rightarrow \infty$ in (56), only the term involving the longitudinal dielectric function remains,

$$-1 = \frac{2q_x}{\pi} \int_0^\infty \frac{dq_z}{q^2 \varepsilon_\ell(q, \omega)}, \quad (57)$$

which, in the hydrodynamic approximation and small wave vectors becomes Ritchie's "classic" result [28]

$$\omega_{sp}(q_x) = \frac{\omega_p}{\sqrt{2}} \left[1 + (a_1 + ia_2)q_x \right], \quad a_1 = \sqrt{\frac{3}{10}} \frac{v_F}{\omega_p}, \quad a_2 = 0. \quad (58)$$

Historic Remark: Before the discovery of the ionosphere, Zenneck and Sommerfeld [34] set-up a theory for the long distance propagation of radio-waves over (conducting) earth or sea-water of just the same type as given by (45-51), (as cited in [31]).

IV. B. Surface-Plasmon Spectroscopy

As the phase-velocity of the surface plasmon is always smaller than the velocity of light in the adjacent dielectric (or vacuum), surface plasmons cannot directly be excited by light. There are, however, two tricks to overcome this problem [29].

- (a) Use of periodic surface structures. If there is a line-grating in the surface with spacing d the photon with frequency ω_0 may pick-up momentum $K_m = 2\pi m/d$, $m = 0, \pm 1, \pm 2, \dots$ from the surface: $q_x = \omega_0 \sin \alpha / c + K_m$. If (q_x, ω_0) is on the dispersion curve, a surface plasmon may be emitted. The latter can decay and, thus, power is absorbed from the reflected beam. Radiative decay with momentum transfer K_n is also possible and lead to additional diffraction peaks which were first observed by Wood[35] as early in 1902. (As cited by Ritchie et al. [36]).
- (b) ATR (attenuated total reflection) or prism method. At the boundary of a dielectric with refractive index n light with frequency ω_0 is totally reflected if the angle of incidence, α , satisfies $\sin \alpha > 1/n$, Fig. 17. In this case, there is an evanescent wave outside the dielectric propagation along the surface with wave-vector $q_x = n(\omega_0/c) \sin \alpha$ in perfect analogy with the surface plasmon. Photons in evanescent waves have $n \sin \alpha$ times larger momentum than in vacuum! The range of accessible wave vectors is $\omega_0/c < q_x < n\omega_0/c$.

Methods using periodic surface structures were first applied to metals where the plasma-frequency is in the UV region. It has not yet been possible to produce grating distances of the same order as the wavelength of light so that only but a small part of the dispersion curve near the light line has been accessible. These experiments, however, have been performed with high accuracy and even then small zone boundary gaps have been observed, Fig. 16. For doped semiconductors, on the other hand, the plasma-frequency is in the IR region and the full excitation curve has been investigated [37].

The ATR technique has two main advantages over the grating technique. (1) The surface of the sample is not destructively disturbed. (2) In the weak coupling limit, i.e. when the gap between the sample and the prism is large enough, the frequencies of the reflectivity minima directly yield the surface plasmon dispersion, Fig. 17.

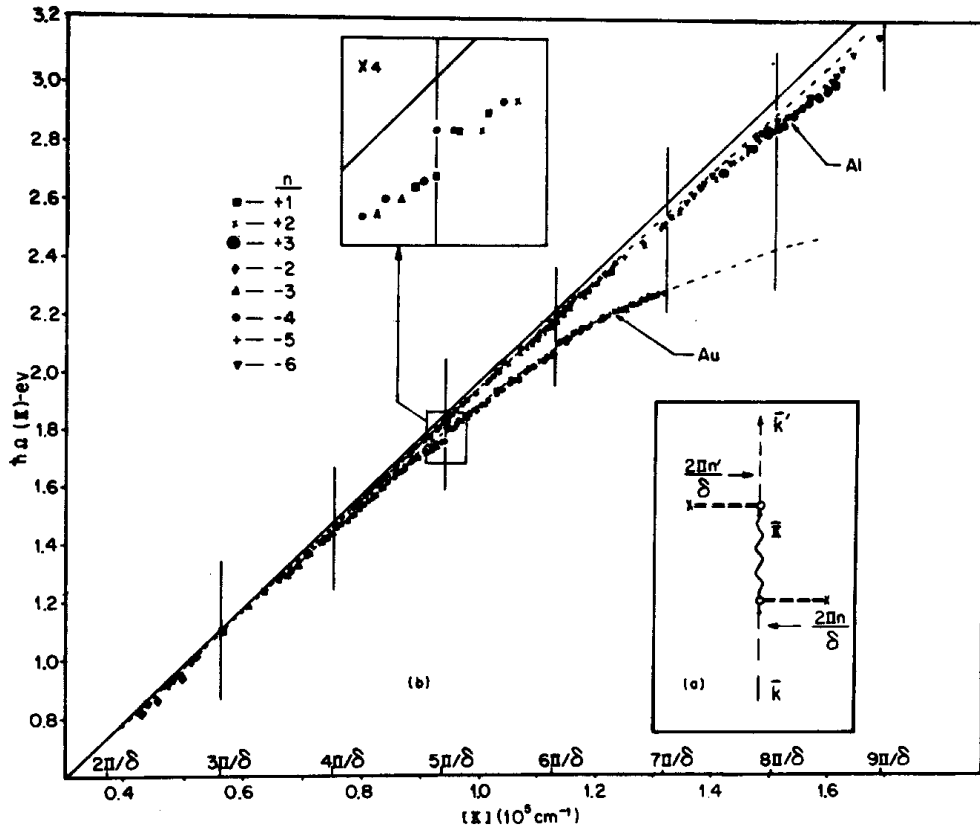


Figure 16. Dispersion curve of surface-plasmons in Al and Au by a concave grating for varying angles between entrance and exit slits. Upper inset shows a zone-boundary gap, lower insets gives a Feynman diagram of the creation and radiative decay of the plasmon. From Ritchie et al. [36]

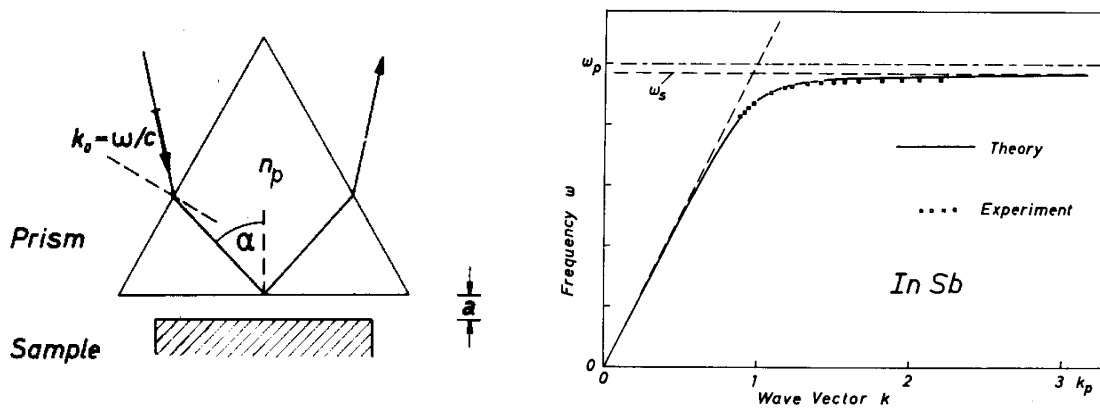


Figure 17. Dispersion of surface plasmons in InSb as obtained from ATR-spectra. $\omega_p = 426.5\text{cm}^{-1}$, $k_p = \omega_p/c$. $\epsilon_\infty = 15.68$, $\gamma = 0.03\omega_p$. From Fischer et al. [37]

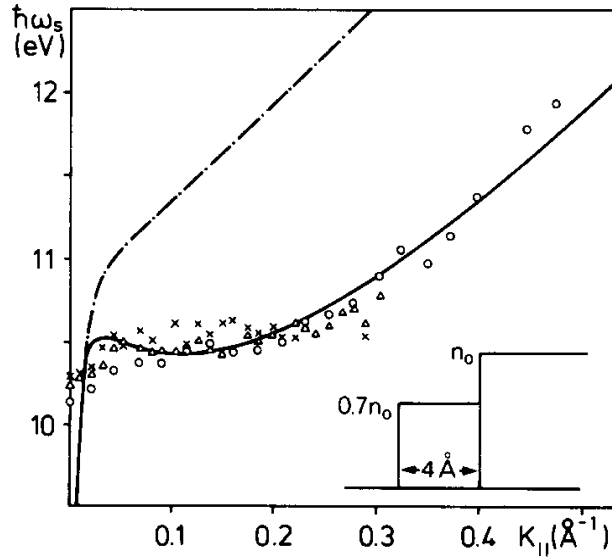


Figure 18. Surface plasmon dispersion of Al. Experimental data from Krane and Raether[39]. The dashed-dotted and solid lines represent the result of a sharp barrier and a two-step model within the hydrodynamic description. From Forstmann and Stenschke[40].

Passage of high energy electrons through a metal has already been discussed in connection with the spectroscopy of bulk-plasmons, however, the influence of the surfaces has been neglected. Fig.7 shows that, at normal incidence, the momentum transferred parallel to the surface is $\hbar q_x = \hbar k_0 \theta$. The angles β and θ are related by

$$\tan \beta = \theta / \theta_{\Delta E}, \quad \theta_{\Delta E} = \Delta E / 2E_0 \quad (59)$$

where E_0 is the kinetic energy of the primary electrons. If θ surpasses $\theta_{\Delta E}$ the angle β quickly approaches 90° so that large q_x are easily possible. However, details of the light-line requires high angular resolution. Here photons are a more suitable tool.

The loss-function for a metal foil of thickness d and area A imbedded in a dielectric with permeability ϵ_b (at normal incidence and neglecting retardation) is [29]

$$P(\mathbf{q}, \omega) \propto \Im \left\{ \frac{-1}{\epsilon(q, \omega) q^2} d + \frac{2q_\perp}{q^4} \frac{[\epsilon(\omega) - \epsilon_b]^2}{\epsilon(\omega) \epsilon_b} A \left[\frac{\sin^2(\frac{\omega d}{2v_0})}{L_+(\omega)} + \frac{\cos^2(\frac{\omega d}{2v_0})}{L_-(\omega)} \right] \right\} \quad (60)$$

with

$$L_+(\omega) = \epsilon(\omega) + \epsilon_b(\omega) \tanh(\frac{q_\perp d}{2}), \quad L_-(\omega) = \epsilon(\omega) + \epsilon_b(\omega) \coth(\frac{q_\perp d}{2}). \quad (61)$$

$q^2 = q_\perp^2 + (\omega/v_0)^2$. ($q_x = q_\perp$). Energy losses inside the (infinite) dielectric boundaries are omitted.

With decreasing film-thickness the surface-modes at both sides become coupled and split into two modes with different frequencies. The zeros of L_\pm define the coupled surface-plasmon frequencies (in the nonretarded limit).

$$\frac{\epsilon_b - \epsilon(\omega)}{\epsilon_b + \epsilon(\omega)} = \mp e^{q_x d}. \quad (62)$$

For a Drude metal imbedded in a dielectric we have for $q_x > \omega_p/c$

$$\omega_\pm(q_x) = \frac{\omega_p}{\sqrt{1 + \epsilon_b}} \sqrt{1 \pm e^{-q_x d}}. \quad (63)$$

The plus/minus sign correspond to a symmetric/antisymmetric mode in which an excess charge at one side of the surface is accompanied by an excess/deficiency of charge just opposite at the other side of the slab. The splitting into two modes can be neglected if $q_x d / 2 > 1$. In the case of 50 keV electrons this condition means $\theta d > 10^{-2}$ (d in \AA and θ in degrees).

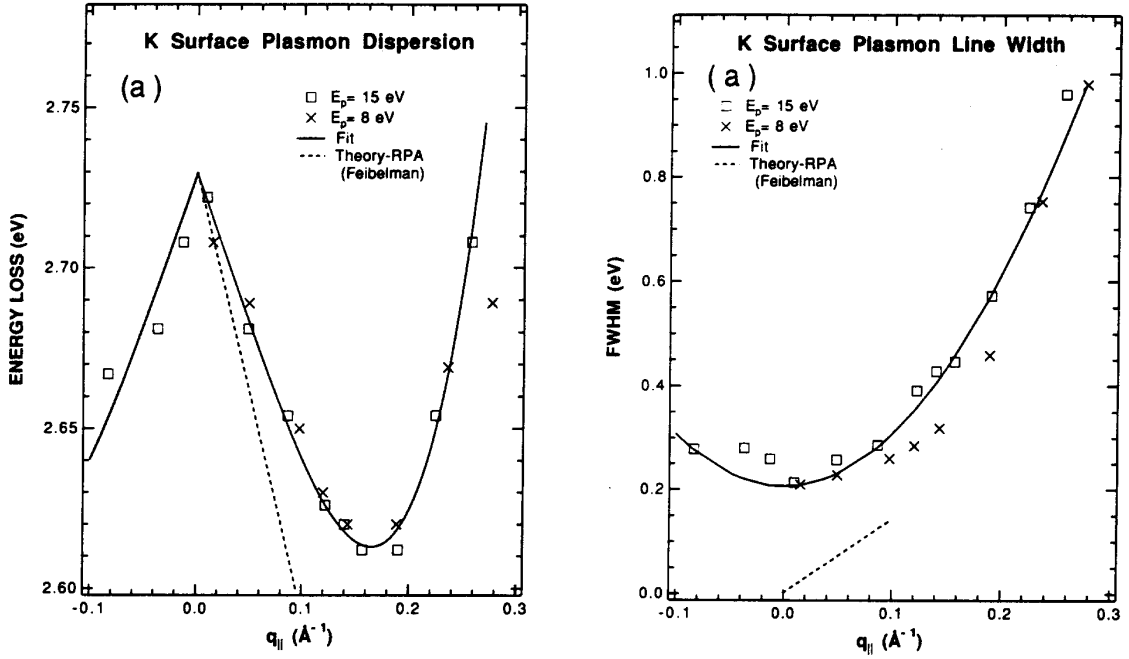


Figure 19. Surface plasmon dispersion (left) and width (right) for Potassium. Data are shown for two different incident electron energies. Dashed Line: Feibelman's theory [44]. From Tsuei et al. [41,44].

Experimental results for *Al* are displayed in Fig. 18. Contrary to the sharp barrier result (58) the expected steep increase is not observed. Bennet[38] was the first who realized that the surface plasmon-dispersion is sensitive to the surface-charge density profile. A “soft” boundary decreases the linear term in (58), which can even become negative.

There is extensive literature devoted to the study of spatial dispersion and a diffuse surface electron profile on the plasmon-dispersion curve at a metal surface. For a survey see [41]. For small wave-vectors (but still $q_x > \omega_p/c$) the surface-plasmon is of the form (58). The coefficient a_1 is the centroid of the induced surface-charge density [42-44].

$$a_1 = -\frac{\int_{-\infty}^{\infty} z \delta\rho(z) dz}{\int_{-\infty}^{\infty} \delta\rho(z) dz}. \quad (64)$$

($\delta\rho(z) = d(z)$, Fig. 15). In the absence of impurities or phonon scattering a_2 results from particle-hole excitations (Landau-damping).

Angle resolved inelastic low-energy electron reflection scattering has been used for alkali films [41,45], Fig. 19. For all alkali metals measured the dispersion coefficient $a_1 < 0$. At the frequency of the surface plasmon oscillation the induced charge is outside of the geometrical boundary, thus, the surface plasmon-dispersion is negative. Feibelman[44] has shown from microscopic considerations that, similar to the nonlocal description in the bulk in term of longitudinal and transverse dielectric functions, nonlocal surface effects can be expressed in terms of two surface response functions $d_{\perp}(\omega)$, $d_{\parallel}(\omega)$ which only depend on frequency. Remarkably, $\omega_{sp}(0)$ does not depend on the surface charge profile and, thus, is a bulk property of the metal.

For *Ag*, on the other hand, $a_1 > 0$ and, a strong azimuthal anisotropy is observed [45-48].

V. PLASMONS IN SMALL PARTICLES AND CLUSTERS

V. A. Multipolar Plasmons

In recent years, small particles have received growing attention because of their interesting physical properties and technical importance. For an overview see e.g. [49]. Concerning the interaction of a transverse, monochromatic plane wave with a single spherical (metallic or dielectric) particle, the basic theory has been developed by Mie and Debye more than 80 years ago [50], see [32]. The analogous problem for longitudinal (electric) fields, however, received attention much later in connection with electron–energy–loss spectroscopy [51].

The system under consideration consists of a metallic sphere of radius R imbedded in a dielectric host with dielectric function $\varepsilon_h(\omega)$. The metal inside the sphere will be either described by the Drude-function with $\varepsilon_D(\omega)$, or within a hydrodynamic theory.

In a local dielectric description the total potential $\phi = \phi_{ind} + \phi_{ext}$ fulfills the Poisson-equation, $\Delta\phi = -\rho_{ext}/\epsilon_0\epsilon$, so that ϕ_{ind} is related to ϕ_{ext} by

$$\phi_{ind}(\mathbf{x}, \omega) = \left(\frac{1}{\epsilon} - 1\right)\phi_{ext} + f(\mathbf{x}, \omega). \quad (65)$$

$f(\mathbf{x}, \omega)$ is a regular solution (except on the surface) of the Laplace-equation, $\Delta f = 0$. In terms of spherical harmonics, this function is represented by

$$f_{\ell m}(r, \omega) = C_1^{\ell m}(\omega) \theta(R - r) \left(\frac{r}{R}\right)^\ell + C_2^{\ell m}(\omega) \theta(r - R) \left(\frac{R}{r}\right)^{\ell+1}. \quad (66)$$

Coefficients C_1 and C_2 are determined by the requirement of continuity of the tangential component of \mathbf{E} and normal component of \mathbf{D} at the surface of the sphere. As a result, we obtain

$$\begin{aligned} r \leq R: \quad \phi_{\ell m}^{ind}(r) &= \frac{\ell+1}{\ell} \alpha_\ell^{c\ell} \epsilon_{met}^{-1} \phi_{\ell m}^{ext}(R) \left(\frac{r}{R}\right)^\ell + \left(\frac{1}{\epsilon_{met}} - 1\right) \phi_{\ell m}^{ext}(r) \\ r \geq R: \quad \phi_{\ell m}^{ind}(r) &= -\alpha_\ell^{c\ell} \epsilon_h^{-1} \phi_{\ell m}^{ext}(R) \left(\frac{R}{r}\right)^{\ell+1} + \left(\frac{1}{\epsilon_h} - 1\right) \phi_{\ell m}^{ext}(r). \end{aligned} \quad (67a, b)$$

The key quantity is the classical multipolar polarizability (divided by $R^{2\ell+1}$)

$$\alpha_\ell^{c\ell}(\omega) = \frac{\epsilon_{met}(\omega) - \epsilon_h(\omega)}{\epsilon_{met}(\omega) + \frac{\ell+1}{\ell} \epsilon_h(\omega)}. \quad (68)$$

$\ell=1,2,\dots$ For a spherical void filled with a dielectric (a noble gas “bubble”) $\epsilon_{met}, \epsilon_h$ have to be interchanged.

The eigenfrequencies of the collective modes can be obtained from the poles of (68). For a metallic particle with a Drude-dielectric function, imbedded in a nondispersive host these modes are known as Mie-resonances.

$$\omega_\ell = \frac{\omega_p}{\sqrt{1 + \frac{\ell+1}{\ell} \epsilon_h}}, \quad (69)$$

As pointed out by Ekardt [52], the classical result has several deficiencies which become important for particle diameters $2R$ in the range of $2nm$ or less. For instance, according to (69) there is always a pronounced dipole resonance at $\omega_1 = \omega_p/\sqrt{1+2\epsilon_h}$, but this structure disappears in a quantum treatment for small radii. For $\ell \rightarrow \infty$, (69) approaches the surface-plasma frequency of an infinite plane metal-vacuum boundary, $\omega_\ell \rightarrow \omega_p/\sqrt{1+\epsilon_h}$, whereas in quantum theory it becomes overdamped and effectively disappears.

A qualitative similar behaviour is obtained in a hydrodynamic description, where the collective excitations are determined by the transcendental equation [53-55]:

$$\frac{j_{\ell+1}(kR)}{j_{\ell-1}(kR)} = \frac{\ell}{\ell+1} \frac{k^2}{k^2 + \kappa^2} \frac{(2\ell+1)\epsilon_h}{(\ell+1)\epsilon_h + \ell} \quad (70)$$

where $j_\ell(x)$ denotes a spherical Bessel-function and

$$k^2 = \beta^{-2}[\omega(\omega + i\gamma) - \omega_p^2], \quad \kappa^2 = \omega_p^2/\beta. \quad (71)$$

The solutions of (70) fall into two classes:

- (a) Surface-modes ($\omega_\ell < \omega_p$, $\ell = 1, 2, \dots$).

These modes correspond to imaginary values of k so that the induced charge density is concentrated near the surface. For large spheres, $j_{\ell+1}/j_{\ell-1} \rightarrow -1$, yielding ω_ℓ of (69). With decreasing sphere-radius, ω_ℓ increases and eventually reaches ω_p at a critical radius R_ℓ and becomes a bulk mode.

- (b) Bulk-modes ($\omega_\alpha > \omega_p$), $\alpha = (l, \nu)$.

k is real and the charge density oscillations are spread over the whole particle volume. For $\ell = 0$, the solution of (70) is given by $kR = x_{1,\nu}$, where $x_{\ell,\nu}$ is the ν^{th} positive root of $j_\ell(x) = 0$. From a graphical discussion, we deduce that the modes of higher multipolarity are lying in the intervals $x_{\ell+1,\nu} \leq kR \leq x_{\ell-1,\nu+1}$. As kR increases from zero to infinity, the left hand side of (70) has first order poles at $x_{\ell-1,\nu}$ whereas the right hand side is positive and finite. The bulk modes are thus labelled by $\ell = 0, 1, \dots$ and an additional index $\nu = 1, 2, \dots$. To a first approximation, we have $kR \approx x_{\ell-1,\nu+1}$, which (for $\ell > 0$ and $R > R_\ell$) leads to

$$\omega_{\ell,\nu} \approx -i\gamma/2 + \omega_p \sqrt{1 + \left(\frac{x_{\ell-1,\nu+1}}{\kappa R}\right)^2 - (\gamma/2\omega_p)^2}. \quad (72)$$

The ℓ, ν dependence of the collective modes is analogue to the bulk-plasmon dispersion. For $\ell = 0$, which is known as the breathing mode $x_{\ell-1,\nu+1}$ is replaced in (72) by $x_{1,\nu}$. In plasma physics the bulk modes are known as Tonks-Dattner resonances [56]. In thin metallic films they can be excited optically by p-polarized light [57] ($\ell \geq 1$).

V. B. Spectroscopy of Cluster-Plasmons and Experimental Results

At present two different experimental techniques are used to study the electronic excitations of small particles: Electron-energy loss spectroscopy (EELS) and scanning transition electron microscopy (STEM) [58]. EELS controls the momentum transfer whereas STEM controls the impact parameter.

In an EELS experiment the scattered electrons excite multipolar modes up to $\ell \approx qR$, where R is the radius of the particles so that the analysis of cluster-loss-spectrum is far more complicated than for plane surfaces. As a result, for the dielectric and hydrodynamic description the loss-functions are [55]:

$$P_{diel}(\mathbf{q}_\perp, \omega) = \frac{e^2}{\pi^2 \hbar v^2 \epsilon_o} \frac{1}{s^2} \Im \left\{ \frac{R^3}{3} \frac{-1}{\epsilon_{met}} + \frac{-1}{\epsilon_h} \int_R^\infty r^2 dr \right. \\ \left. + R^3 \left(\frac{1}{\epsilon_h} - \frac{1}{\epsilon_{met}} \right) \sum_{\ell=1}^\infty (2\ell+1)(\ell+1) \frac{\epsilon_{met} - \epsilon_h}{\epsilon_{met} + \frac{\ell+1}{\ell} \epsilon_h} \left[\frac{j_\ell(sR)}{sR} \right]^2 \right\}. \quad (73)$$

$s = |\mathbf{q}| = \sqrt{q_\perp^2 + \left(\frac{\omega}{v}\right)^2}$. v is the electron velocity. In (73) ϵ_{met} and ϵ_h may have arbitrary frequency dependencies. An approximate result has been given before by Ashley and Ferrell [59]. For void in a metal the loss function is simply obtained from (73) by interchanging ϵ_h and ϵ_m .

$$P_{hydro}(\mathbf{q}_\perp, \omega) = \frac{e^2}{\hbar \pi^2 v^2 \epsilon_o s^2} \Im \left\{ \frac{R^3}{3} \frac{-1}{\epsilon(s, \omega)} + \frac{-1}{\epsilon_h} \int_R^\infty r^2 dr \right\} + \\ + \frac{e^2}{\hbar \pi^2 v^2 \epsilon_o} \Im \left\{ \left(\frac{1}{\epsilon(s, \omega)} - 1 \right)^2 \frac{kR^2}{\kappa^2 s^3} \sum_{\ell=0}^\infty (2\ell+1)^2 \times \frac{s j_\ell(kR) j_{\ell-1}(sR) - k j_{\ell-1}(kR) j_\ell(sR)}{J_\ell} \times \right. \\ \left. \times \left(\frac{1}{\epsilon_h} \frac{\ell}{\ell+1} j_{\ell-1}(sR) - \frac{1}{\epsilon_D} j_{\ell+1}(sR) + \frac{s^3}{k^3} \frac{\epsilon_h - 1}{\epsilon_h} \ell \frac{1}{kR} j_\ell(sR) \right) \right\} + \\ + \frac{e^2}{\hbar \pi^2 v^2 \epsilon_o} \Im \left\{ \left(\frac{1}{\epsilon_h} - 1 \right) \frac{R^2}{s^3} \sum_{\ell=0}^\infty (2\ell+1)^2 \frac{j'_\ell(kR)}{J_\ell} j_\ell(sR) \times \left(\frac{1}{\epsilon_h} \frac{\ell}{\ell+1} j_{\ell-1}(sR) - \frac{1}{\epsilon_D} j_{\ell+1}(sR) \right) \right\} \quad (74)$$

$\epsilon(s, \omega)$ denotes the longitudinal wave-vector dependent dielectric function of the bulk metal in hydrodynamic approximation (23). The first and second terms of (73,74) within the curly brackets represent the contributions inside and outside the particle, whereas the other terms describes surface excitations.

Results for potassium clusters in *MgO* are displayed in Figs. 20. (The loss functions have been divided by the prefactor of (73) and $R^3/3$ so that the result is dimensionless). Experimentally, the volume-plasmon half-width of $\hbar\gamma = 0.6$ eV [60] is considerably enhanced in comparison to its bulk value (0.24 eV) [15]. In contrast to the dielectric description, the maxima of the loss function show a considerable “blue-shift”, originating from spatial dispersion for small radii which is in qualitative agreement with the experiment. The bulk-plasmon modes of higher polarity are resolved only in very small particles and for low damping.

For large radii, $R \rightarrow \infty$, the loss-functions (73,74) converge to their infinite medium results (when averaged on the incident directions): On the other side, for small radii or small momentum transfer, $sR \rightarrow 0$, we obtain:

$$P(q_{\perp}, \omega) = \frac{e^2}{4\pi\hbar v^2 \epsilon_0} \frac{V}{s^2} \Im \left[\frac{3}{\epsilon_h} \alpha_1(\omega) \right], \quad (75)$$

$\alpha_1(\omega)$ denotes the (electrical) dipole-polarizability.

Collective excitations on voids or noble gas bubbles in metals have also attracted experimental as well as theoretical interest, e.g. [61-64].

The size-dependence of the surface-plasmon is still an open problem. In the past there was a general agreement that the observed red-shift (with decreasing size) is due to the spill-out of the charge density whereas theories based on sharp surfaces gave a blue-shift. For clusters imbedded in a dielectric host or voids filled with a dielectric, the spill-out is reduced by the exclusion principle so that the assumption of a fixed boundary condition seems to be well-justified. For small metallic particles in vacuum the correct surface charge density profile must be taken into account and clusters eventually require a full self-consistent quantum treatment[65].

How many metal atoms are needed to form a cluster which displays metallic behaviour? For *Hg* 25 atoms seem to be enough! [66-67], Fig. 21. The *Hg* atom has a $5d^{10}6s^2$ closed shell electronic structure so that small clusters are dominantly van der Waals bound. The width of the occupied $6s$ and empty $6p$ bands increase roughly proportional to the number of nearest neighbors. Thus the band gap decreases for increasing cluster size and becomes zero around $N = 20$.

For *Na* the evolution towards the bulk values of the plasmons in clusters comprising from 8 to 338 atoms has been calculated by Yannouleas et al [68] who found an increase of the Mie-plasmon energy from 2.7 to 3.2eV. The latter value is close to $\omega_p/\sqrt{3}$.

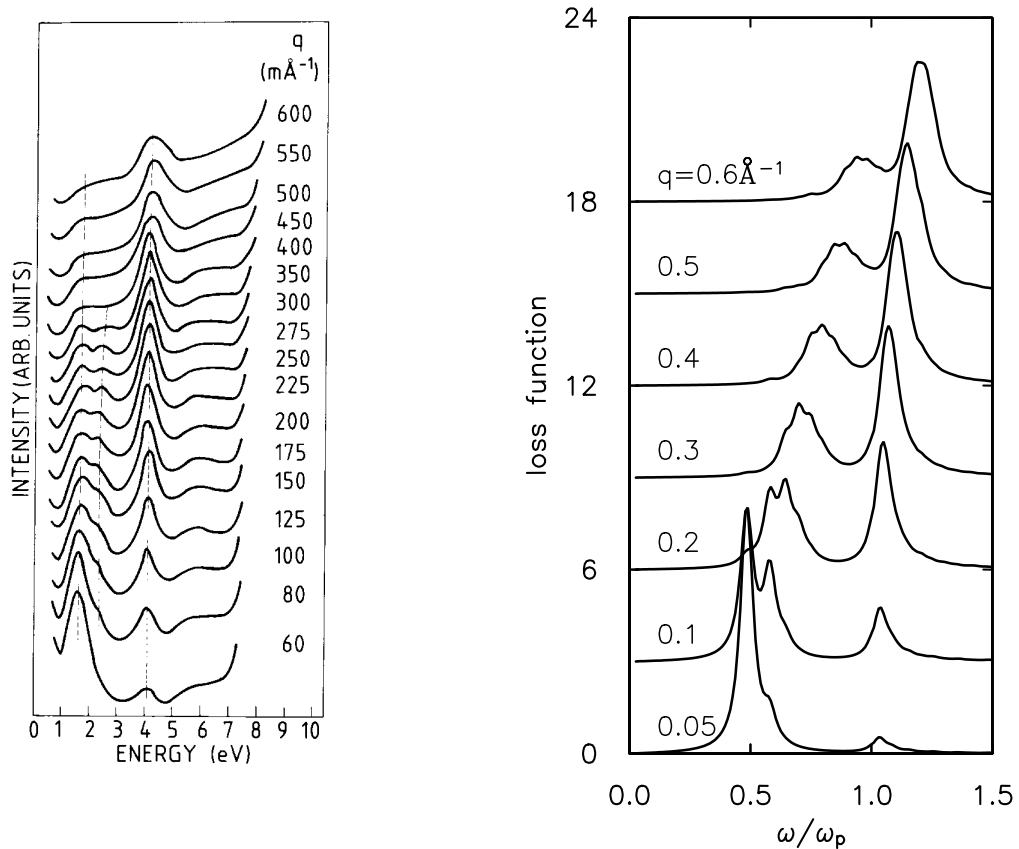


Figure 20. Energy-loss spectrum of K-clusters in MgO [60]. (Left) experimental results, (right) hydrodynamic theory (74). Particle radius: $R = 20\text{\AA}$.

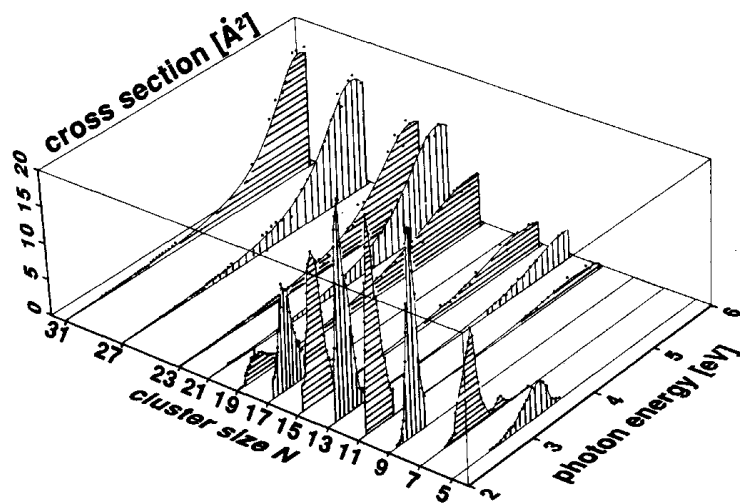


Figure 21. Experimental Photoabsorption spectra of doubly charged Hg clusters showing an abrupt transition from atomic to collective, plasmon-like absorption as a function of cluster size. From Haberlandt et al. [66].

VI. HETROSTRUCTURES AND LOW-DIMENSIONAL SYSTEMS

A metallic heterostucture is an arrangement of different metals in close contact, i.e. an array of metallic sheets in which there is a negligible charge transfer between the components. In the limit of thick enough layers, one can treat the layers individually by Drude dielectric functions (23) or hydrodynamic equations (10). Typically the thickness of the individual layers lies in the range $100 \dots 5000 \text{ \AA}$. These structures resemble semiconductor quantum-wells but little work by both theory and experiment appears to have been done on their metallic counterparts.

VI. A. Interfaces

The simplest heterostructure consists of two semi-infinite metals bounding together just in the same way as it was studied for the surface-plasmon in chapter IV. Apart from the bulk and surface plasmons in each metal there is an interface-plasmon whose dispersion is given by (51) where $\varepsilon_{\pm}(\omega)$ are both Drude-functions with bulk-plasma frequencies $\omega_{p\pm}$, Fig. 22. Neglecting retardation the frequency of the interface-plasmon is given by

$$\omega_{int} = \sqrt{\frac{\omega_{p+}^2 + \omega_{p-}^2}{2}}. \quad (76)$$

For small $q_x \rightarrow 0$ $\omega = \omega_{p-} < \omega_{p+}$. Experimental studies on interface-plasmon excitations in *Cu/RbF/GaAs* and *Cu/Rb/Ge* heterostructures were reported by Klauser et al. [69].

VI. B. Sandwich-Configurations

A metallic slab or foil of thickness d and dielectric function $\varepsilon(\omega)$ imbedded in a metallic host with dielectric function $\varepsilon_h(\omega)$ displays two interface modes with dispersions $\omega_{\pm}(q_x)$, Fig. 23. The plus/minus sign correspond to a symmetric/antisymmetric configuration of induced charges at the interfaces. Neglecting retardation as well as spatial dispersion these modes are determined by the zeros of $L_{\pm}(\omega)$ of (61)

$$L_+(\omega) = \varepsilon(\omega) + \varepsilon_h(\omega) \tanh\left(\frac{q_x d}{2}\right) = 0, \quad L_-(\omega) = \varepsilon(\omega) + \varepsilon_h(\omega) \coth\left(\frac{q_x d}{2}\right) = 0. \quad (77)$$

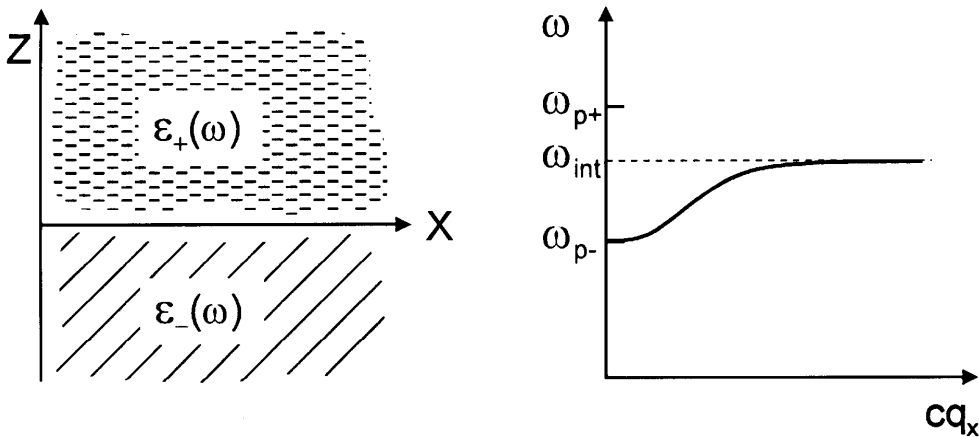


Figure 22. Geometry (left) and interface-plasmon dispersion (right) of a metal-metal contact.

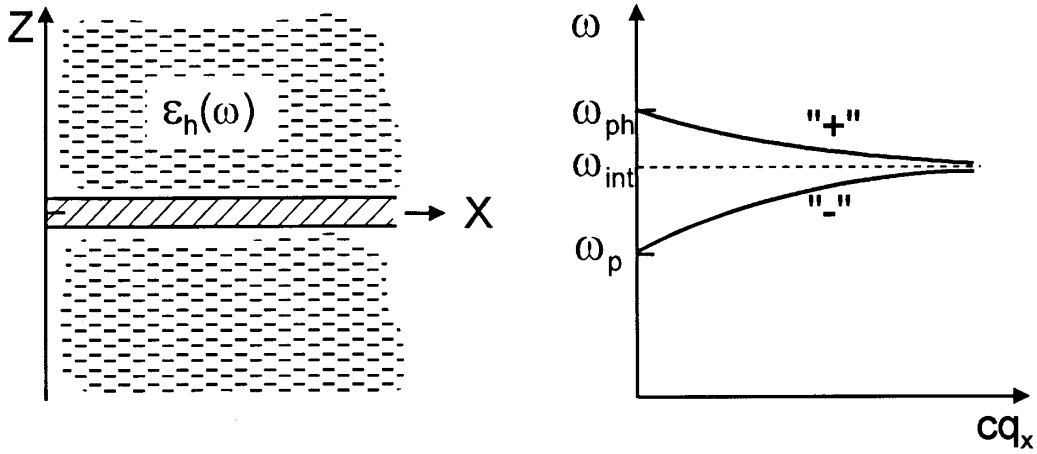


Figure 23. Geometry (left) and interface-plasmon dispersions (right) of a metallic sandwich.

VI. C. Two-Dimensional Systems

Ritchie [28] first noted that the plasmon in a thin sheet has a square-root dispersion ($d \rightarrow 0$ for the “-” mode (77)). Stern [70] later derived the explicit dispersion relation for the 2D plasmon (in the nonretarded limit but including spatial dispersion)

$$\omega_{2D}(q_x) = \sqrt{\frac{N_s e^2}{2m^* \epsilon_0 \bar{\epsilon}(\mathbf{q}, \omega)}} q_x, \quad (78)$$

where N_s is the areal carrier density and $\bar{\epsilon}$ is an effective dielectric function. For a MOS configuration consisting of a semiconductor with dielectric constant ϵ_{sc} , an (SiO_2 -oxide) insulator with ϵ_{ox} and thickness d , and a perfectly screening gate

$$\bar{\epsilon}(q_x, \omega) = \frac{1}{2} [\epsilon_{sc}(\omega) + \epsilon_{ox}(\omega) \coth(dq_x)]. \quad (79)$$

Such 2D-plasmons have been observed in $AlGaAs-GaAs$ heterostructures where the electrons are confined in a very narrow potential well, see e.g. Heitmann [71], or Wilkinson et al. [72].

VI. D. Two-Layer Systems

In a layered electron gas, the free charges are constrained to move on parallel planes spaced by a distance d . Such a two-layer system was studied by Olego et al. [73] and Yuh et al. [74]. Here, the plasmon-dispersion relation is quite different from that in 2D or 3D plasmas

$$\omega(\mathbf{q}) = \sqrt{\frac{N_s e^2}{2\epsilon_0 \epsilon_M m^*} \frac{\sinh(q_{\parallel})}{\cosh(q_{\parallel}d) - \cos(q_{\perp}d)}}. \quad (80)$$

ϵ_M is the dielectric constant supporting the planes and $q_{\parallel} = q_x$ and q_{\perp} are the in-plane and normal components of wave vector \mathbf{q} . For large separations $q_{\parallel}d \gg 1$ the dispersion reduces to that of a 2D plasma. For $q_{\parallel}d \ll 1$ the planes oscillate in phase and the dispersion is 3D like. However, when $q_{\perp} \neq 0$ the contributions from the induced fields in different planes tend to cancel. Then (80) takes the distinctive linear dependence

$$\omega(\mathbf{q}) = q_{\parallel} \sqrt{\frac{N_s e^2}{2\epsilon_0 \epsilon_M m^*} \frac{d}{1 - \cos(q_{\perp}d)}}. \quad (81)$$

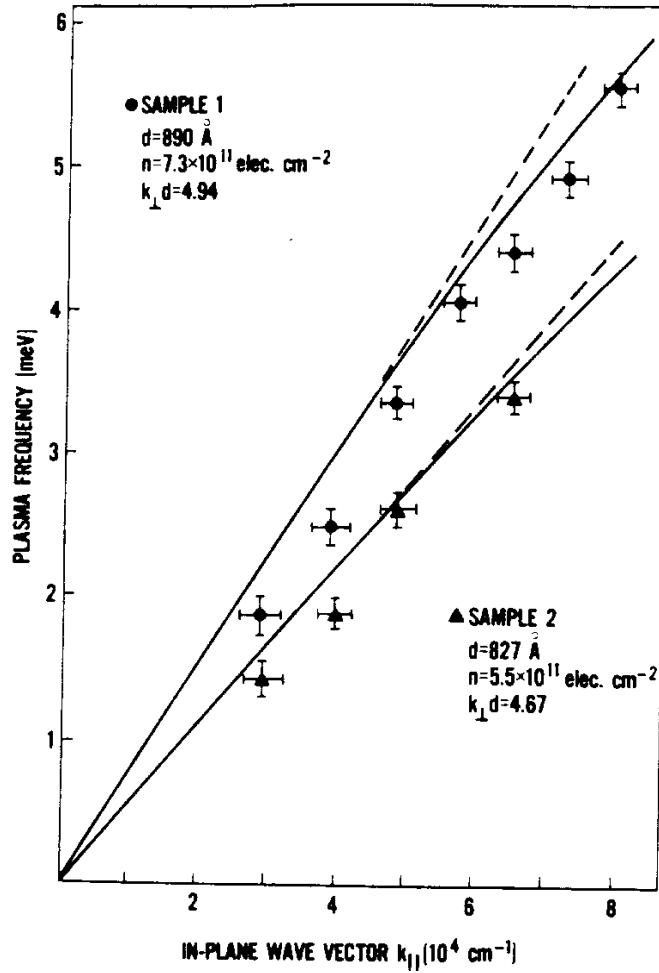


Figure 24. Dispersion relation for a two-layer plasma in *GaAs - AlGaAs* heterostructures. Solid and dashed lines are evaluations of (80) and (81), respectively. From Olego et al. [73].

In this regime ($q_{\parallel} d \ll 1$, $q_{\perp} \neq 0$) the response is most different from that in 2D or 3D plasmas, Fig. 24.

VI. E. Superlattices

Superlattices are structures composed of alternating layers of different materials, Fig. 25. Theoretical studies on superlattice plasmons and their spectroscopy were reported e.g. by Babiker [75], Shi and Griffin [76], and Lopez-Olazagasti et al. [77].

More recently the theory of infinite metallic superlattices has found a new application in the study of high T_c superconductors. These can be viewed as periodic arrays of unit cells with a typical spacing of about 12 \AA , each of which contains up to three closely spaced CuO_2 sheets. Even at these small separations, the electronic bands are 2D like [78,79].

ACKNOWLEDGEMENT

I thank Prof. J. Fink for many stimulating and helpful discussions.

APPENDICES

A.1 Hydrodynamic Description

Following Bloch [80] and Jensen [81], the state of the plasma is described by the density and velocity fields $n(\mathbf{r}, t)$, $\mathbf{v}(\mathbf{r}, t)$, respectively. For the longitudinal response the velocity field is irrotational, $\mathbf{v}(\mathbf{r}, t) = -\text{grad}\Psi(\mathbf{r}, t)$, where $\Psi(\mathbf{r}, t)$ denotes the velocity potential. The equations of motion can be derived from the action principle

$$\delta S = 0, \quad S[n, \Psi] = \int L[n(\mathbf{r}, t), \Psi(\mathbf{r}, t)] dt \quad (\text{A1.1})$$

with Lagrangian L and Hamiltonian H

$$L[n, \Psi] = m_0 \int n(\mathbf{r}, t) \frac{\partial \Psi}{\partial t} d\mathbf{r} - H \quad (\text{A1.2})$$

$$H = \frac{m_0}{2} \int n(\mathbf{r}) [\text{grad}\Psi(\mathbf{r})]^2 d\mathbf{r} - e \int \Phi_+(\mathbf{r}) n(\mathbf{r}) d\mathbf{r} + \frac{1}{2} \frac{e^2}{4\pi\epsilon_0} \int \int \frac{n(\mathbf{r})n(\mathbf{r}')}{|\mathbf{r} - \mathbf{r}'|} d\mathbf{r}d\mathbf{r}' + E_0[n(\mathbf{r})] \quad (\text{A1.3})$$

where $E_0[n]$ is the (exact) ground state energy of the interacting electron gas at (local) density $n(\mathbf{r})$ and $\Phi_+(r)$ is the potential of the positive ion background.

We are interested in the small density oscillations of the plasma around its equilibrium density n_0 . Correspondingly, we expand $H[n, \Psi]$ around its minimum at $n = n_0$, $\Psi = 0$. Therefore, this expansion begins with quadratic terms in $n_1 = n - n_0$:

$$H = H_0 + \frac{m_0}{2} \int n_0 [\text{grad}\Psi(\mathbf{r})]^2 d\mathbf{r} + \frac{1}{2} \frac{e^2}{4\pi\epsilon_0} \int \int \frac{n_1(\mathbf{r})n_1(\mathbf{r}')}{|\mathbf{r} - \mathbf{r}'|} d\mathbf{r}d\mathbf{r}' + \frac{1}{2} \int \frac{\partial^2 E_0[n_0]}{\partial n_0^2} n_1^2(\mathbf{r}) d\mathbf{r} \dots \quad (\text{A1.4})$$

Variation with respect to $n_1(\mathbf{r}, t)$ and $\Psi(\mathbf{r}, t)$, leads to

$$m_0 \frac{\partial \Psi(\mathbf{r}, t)}{\partial t} + e\phi_1(\mathbf{r}, t) - P_0 n_1(\mathbf{r}, t) = 0, \quad \frac{d}{dt} [m_0 n_1(\mathbf{r}, t)] - m_0 \text{div} [n_0 \text{grad}\Psi(\mathbf{r}, t)] = 0 \quad (\text{A1.5})$$

with

$$\Delta\phi_1(\mathbf{r}, t) = -\frac{1}{\epsilon_0} (-e)n_1(\mathbf{r}, t), \quad P_0 = \frac{\partial^2 E_0[n_0]}{\partial n_0^2}. \quad (\text{A1.6})$$

In a local Hartree-Fock approximation (5)

$$E_0[n(\mathbf{r})] = \int \left[\frac{3}{5} \epsilon_F [n(\mathbf{r})] - \frac{3}{4\pi} e^2 k_F [n(\mathbf{r})] \right] n(\mathbf{r}) d\mathbf{r} \quad (\text{A1.7})$$

we obtain for the plasmon dispersion-coefficient

$$\beta = \frac{m_0}{n_0} P_0 = \frac{1}{3} v_F^2 - \frac{1}{3\pi} \frac{e^2 k_F}{m_0}. \quad (\text{A1.8})$$

As already noted in chapter 2, (A1.8) is not quantitatively correct so that β will be used as a parameter to fit the experimental plasmon-dispersion. The reason of this discrepancy lies in the roots of the hydrodynamic description itself which is correct for small q, ω , whereas, plasmons are a high frequency phenomenon. Nevertheless, the description is based on conservation laws and contains the essential physics.

A2. Kinetic Theory

In a kinetic description the state of a (one-component) plasma is described by a phase-space distribution function $f(\mathbf{r}, \mathbf{p}, t)$ which obeys the Boltzmann-Vlasov equation [82]

$$\frac{\partial f}{\partial t} + \mathbf{v} \frac{\partial f}{\partial \mathbf{v}} + \mathbf{F} \frac{\partial f}{\partial \mathbf{p}} = I(f). \quad (\text{A2.1})$$

\mathbf{v} is the velocity of the particles with energy-momentum relation $\epsilon(\mathbf{p})$ and $\mathbf{F} = -e(\mathbf{E} + \mathbf{v} \times \mathbf{B})$ is the Lorentz-force. For isotropic and elastic (impurity-) scattering the collision integral becomes

$$I(f) = \frac{1}{\tau} \left(\langle f \rangle_{\Omega} - f \right), \quad \langle f \rangle_{\Omega} = \frac{1}{4\pi} \int f(\mathbf{r}, \mathbf{p}, t) d\Omega_p, \quad (\text{A2.2})$$

where τ is the scattering time and $\langle \dots \rangle$ denotes the angular average on the momentum directions.

Eq(A2.1) must be jointly solved with the Maxwell-equations which, in the quasistatic approximation, reduce to

$$\mathbf{E}(\mathbf{r}, t) = -\text{grad}\Phi(\mathbf{r}, t), \quad \Delta\Phi(\mathbf{r}, t) = -\frac{1}{\epsilon_0} [\rho_+ - en(\mathbf{r}, t) + \rho_{ext}(\mathbf{r}, t)], \quad (\text{A2.3})$$

where $n(\mathbf{r}, t)$ is the electron-density

$$n(\mathbf{r}, t) = \frac{2}{(2\pi\hbar)^3} \int f(\mathbf{r}, \mathbf{p}, t) d^3\mathbf{p}. \quad (\text{A2.4})$$

Next we consider small perturbations by the external field, $\Delta\Phi_{ext} = -\rho_{ext}/\epsilon_0$,

$$f = f_0 + f_1, \quad n(\mathbf{r}, t) = n_0 + n_1(\mathbf{r}, t). \quad (\text{A2.5})$$

$f_0(\epsilon(\mathbf{p}))$ is the Fermi-function and n_0 is the equilibrium electron density. In linearized form, (A2.1) can be solved by Fourier-transformation with respect to t, \mathbf{r} , see e.g. [27]

$$-i\omega f_1(\mathbf{q}, \mathbf{p}, t) + i\mathbf{v}\mathbf{q}f_1(\mathbf{q}, \mathbf{p}, t) + ie\mathbf{q}\Phi \frac{\partial f_0}{\partial \epsilon_p} \mathbf{v} = I(f_1). \quad (\text{A2.6})$$

In particular, in the absence of collisions ($\tau = \infty$), we obtain:

$$f_1(\mathbf{q}, \mathbf{p}, t) = -e\Phi(\mathbf{r}, t) \frac{\partial f_0}{\partial \epsilon_p} \frac{\mathbf{q}\mathbf{v}_p}{\mathbf{q}\mathbf{v}_p - \omega}, \quad \Phi(\mathbf{q}, \omega) = -\frac{e}{\epsilon_0 q^2} n_1(\mathbf{q}, \omega). \quad (\text{A2.7})$$

From (A2.5)

$$n_1(\mathbf{q}, \mathbf{p}, t) = \frac{em_0 p_F}{\pi^2 \hbar^3} \left\{ 1 - \frac{\omega}{2qv_F} \ln \left[\frac{1 + \left(\frac{qv_F}{\omega}\right)}{1 - \left(\frac{qv_F}{\omega}\right)} \right] \right\}. \quad (\text{A2.8})$$

Exchange and correlation effects can be included in the same way as in appendix A1 (yet the kinetic energy has to be left-out)

$$-e\Phi \rightarrow -e\Phi + \frac{\delta^2 E_{xc}[n]}{\delta n_0^2} n_1. \quad (\text{A2.9})$$

Near $q = 0$ the plasmon dispersion is given by

$$\omega^2 = \omega_p^2 + \left[\frac{3}{5} v_F^2 + \frac{n}{m} \frac{\delta^2 E_{xc}[n]}{\delta n_0^2} \right] q^2 + \dots \quad (\text{A2.10})$$

In a standard local density approximation [11]

$$E_{xc}[n(\mathbf{r})] = \int \varepsilon_{xc}[n(\mathbf{r})] n(\mathbf{r}) d\mathbf{r}, \quad (\text{A2.11})$$

$$\varepsilon_{xc}[n(\mathbf{r})] = \frac{-0.916}{r_s} - 0.045 \left[(1 + x^3) \ell n(1 + \frac{1}{x}) + \frac{x}{2} - x^2 - \frac{1}{3} \right].$$

r_s is the density parameter and $x = r_s/21$. As a result we obtain for the q^2 -coefficient defined by (37), (A2.10)

$$\frac{\alpha}{\alpha_{RPA}} = 1 - \left[0.092r_s + \frac{0.0034r_s^2}{1 + r_s/21} \right] \quad (\text{A2.12})$$

agrees very well with the Vashishta and Singwi' result [16]. For $r_s = 6$, $\alpha/\alpha_{RPA} = 0.35$ and $\alpha = 0$ at $r_s = 8.83$. Nevertheless, the experimental dispersion coefficient shows a much stronger r_s -dependence as given by (A2.12).

As a result we obtain for the longitudinal and transverse dielectric functions (without exchange and correlation effects but including collisions)[27,57]

$$\begin{aligned}\varepsilon_\ell(\mathbf{q}, \omega) &= 1 - \frac{\omega_p^2}{\omega(\omega + i\gamma)} \frac{3}{a^2} \left(1 - \frac{\tan^{-1} a}{a}\right) \left[1 + i\frac{\gamma}{\omega} \left(1 - \frac{\tan^{-1} a}{a}\right)\right]^{-1}, \\ \varepsilon_t(\mathbf{q}, \omega) &= 1 - \frac{\omega_p^2}{\omega(\omega + i\gamma)} \frac{3}{2a^2} \left(\frac{1 + a^2}{a} \tan^{-1} a - 1\right)\end{aligned}\quad (A2.13)$$

with abbreviations

$$a^2 = -\frac{\mathbf{q} \cdot \mathbf{q} v_F^2}{(\omega + i\gamma)^2}, \quad \tan^{-1} z = \frac{1}{2i} \ln \left(\frac{1 + iz}{1 - iz}\right). \quad (A2.14)$$

(A2.13) hold even for complex wave-vectors, $Im a \geq 0$, $\ln(1) = 0$.

A3. Quantum Self-Consistent-Field-Approximation (SCFA)

In the self consistent field approximation, the response of the interacting electrons to a weak (scalar) external potential $\Phi_{ext}(\mathbf{r}, t)$ is approximated by a system of noninteracting electrons, responding to the total potential $\Phi = \Phi_{ext} + \Phi_{ind}$ [2,83].

$$\hat{\mathbf{H}} = \frac{\hat{\mathbf{p}}^2}{2m_0} + U(\mathbf{r}, t) + V(\mathbf{r}, t) \quad (A3.1)$$

where $U(\mathbf{r}, t)$ is the periodic crystal potential and $V(\mathbf{r}, t) = -e\Phi(\mathbf{r}, t)$. The microscopic dielectric ($\hat{\varepsilon}$ -operator) is defined through

$$V = \hat{\varepsilon}^{-1} V_{ext}, \quad V_{ext} = \hat{\varepsilon} V \quad (A3.2)$$

In particular we consider a monochromatic external potential with wave-vector \mathbf{Q} and frequency ω

$$V_{ext}(\mathbf{r}, t) = V_{ext}(\mathbf{Q}, \omega) e^{i(\mathbf{Q}\mathbf{r} - \omega t)} + cc, \quad (A3.3)$$

where $\mathbf{Q} = \mathbf{q} + \mathbf{G}$ and \mathbf{q} is within the first Brillouin-zone and \mathbf{G} is a vector of the reciprocal lattice. Due to the periodicity of the crystal potential the induced charge distribution additionally includes contributions from other reciprocal lattice vectors even if \mathbf{Q} is small (so-called local field contributions),

$$V_{ind}(\mathbf{r}, t) = V_{ind}(\mathbf{Q}, \omega) e^{i(\mathbf{Q}\mathbf{r} - \omega t)} + \sum_{\mathbf{G}' \neq \mathbf{G}} V_{ind}(\mathbf{Q}', \omega) e^{i(\mathbf{Q}'\mathbf{r} - \omega t)} + cc. \quad (A3.4)$$

$\mathbf{Q}' = \mathbf{q} + \mathbf{G}'$. Reasoning along the same lines, the total potential in (A3.1) is coupled to the external potential by (A3.2) which becomes a matrix equation

$$\Phi_{ext}(\mathbf{q} + \mathbf{G}, \omega) = \sum_{\mathbf{G}'} \varepsilon_{\mathbf{G}\mathbf{G}'}(\mathbf{q}, \omega) \Phi(\mathbf{q} + \mathbf{G}', \omega). \quad (A3.5)$$

For a crystal $\varepsilon_{\mathbf{G}\mathbf{G}'}(\mathbf{q}, \omega)$ is the analogue of the Jellium $\varepsilon_\ell(\mathbf{q}, \omega)$.

Four steps are necessary to obtain the microscopic dielectric matrix [84,85]:

- (a) First, the correction of the electron density operator is calculated to first order in the total field $V(\mathbf{r}, t)$, $\hat{\rho} = \hat{\rho}_0 + \hat{\rho}_1$, where $\hat{\rho}_0$ describes thermal equilibrium.
- (b) The induced charge density is obtained from $n_1(\mathbf{r}, t) = Sp[\hat{\rho}_1(t)\delta(\mathbf{r} - \hat{\mathbf{r}})]$.
- (c) Poisson equation $\Delta\Phi_{ind} = en_1(\mathbf{r}, t)/\epsilon_0$.
- (d) $\Phi_{ind}[\Phi]$ is a (linear) functional of the total potential. When writing $\Phi = \Phi_{ind} + \Phi_{ext}$ in the form of (A3.5) the dielectric matrix can be read-off as

$$\varepsilon_{\mathbf{G}\mathbf{G}'}(\mathbf{q}, \omega) = \epsilon_\infty \delta_{\mathbf{G}\mathbf{G}'} - \frac{e^2}{\epsilon_0 \Omega |\mathbf{q} + \mathbf{G}|^2} \sum_{\alpha\alpha'} \frac{f(E_\alpha) - f(E_{\alpha'})}{E_\alpha - E_{\alpha'} - \hbar(\omega + i\delta)} \langle \alpha | e^{-i\mathbf{Q}'\mathbf{r}} | \alpha' \rangle \langle \alpha' | e^{i\mathbf{Q}\mathbf{r}} | \alpha \rangle \quad (A3.6)$$

Ω is the crystal volume and ϵ_∞ accounts for core-states not explicitly contained in states numbered by α . For Bloch electrons $\alpha = (n, \mathbf{k})$, where n denotes the band index and \mathbf{k} the wave-number. For a review see Sturm [86].

In an EELS-experiment the observed response $V(\mathbf{q} + \mathbf{G})$ has the same Fourier-components as the perturbation $V_{ext}(\mathbf{q} + \mathbf{G})$. It is convenient to define a macroscopic dielectric function

$$[\epsilon_{macro}(\mathbf{q} + \mathbf{G}, \omega)]^{-1} = [\hat{\epsilon}^{-1}]_{\mathbf{G}\mathbf{G}}(\mathbf{q}, \omega). \quad (A3.7)$$

If local field effects are neglected

$$\epsilon_{macro}(\mathbf{q} + \mathbf{G}, \omega) \approx \epsilon_{\mathbf{G}\mathbf{G}}(\mathbf{q}, \omega) \quad (A3.8)$$

(A3.6) leads to the Ehrenreich-Cohn result [83]. For free electrons the Lindhard-function (see [2,5]) is obtained

$$\epsilon_L(\mathbf{q}, \omega) = 1 + \frac{3}{16x^3} \left(\frac{\hbar\omega_p}{E_F} \right)^2 \left\{ 2x + \left[1 - \left(\frac{y-x^2}{2x} \right)^2 \right] \ln \left[\frac{y-x^2-2x}{y-x^2+2x} \right] - \left[1 - \left(\frac{y+x^2}{2x} \right)^2 \right] \ln \left[\frac{y+x^2-2x}{y+x^2+2x} \right] \right\}, \quad (A3.9)$$

where $x = q/k_F$ and $y = \hbar(\omega + i\delta)/E_F$. Explicit forms for the real and imaginary parts may be found, e.g. in [2,4].

According to translational symmetry of the interacting electron gas, momentum is conserved and $\epsilon_\ell(0, \omega) = 1 - (\omega_p/\omega)^2$ is an exact result. Therefore, the plasma frequency as given by (1) is the exact bulk-plasmon frequency for Jellium at $q = 0$. (A3.9) is identical with the random phase approximation (RPA) which was worked out by Bohm and Pines (see [2]) to solve the equation of motion of the density operator.

It is well known that the effects of collisions in a degenerate electron gas cannot be taken into account merely by replacing ω by $\omega + i\gamma$ in the (collisionless) Lindhard function (A3.9). According to Mermin [87] the correct procedure is

$$\epsilon_M(\mathbf{q}, \omega) = 1 + \frac{(1 + i\gamma/\omega)[\epsilon_L(q, \omega + i\gamma) - 1]}{1 + (i\gamma/\omega)[\epsilon_L(q, \omega + i\gamma) - 1]/[\epsilon_L(\mathbf{q}, \omega) - 1]}. \quad (A3.10)$$

Because of the complexity of the many body problem, knowledge of the exact dielectric function is still lacking. Approximate forms for the dielectric function are commonly written as

$$\epsilon_L(\mathbf{q}, \omega) = 1 - \frac{v(\mathbf{q})\chi_0(\mathbf{q}, \omega)}{1 + v(\mathbf{q})G(\mathbf{q}, \omega)\chi_0(\mathbf{q}, \omega)}, \quad (A3.10)$$

where $v(\mathbf{q}) = e^2/\epsilon_0 q^2$ is the Fourier-transform of the Coulomb potential, $\chi_0(\mathbf{q}, \omega)$ is the Lindhard-susceptibility (of the noninteracting electron gas), $\epsilon_\ell(\mathbf{q}, \omega) = 1 - v(\mathbf{q})\chi_0(\mathbf{q}, \omega)$, and $G(\mathbf{q}, \omega)$ is the so-called ‘‘local field function’’. The latter describes the short-range exchange and correlation effects which are responsible for the local depletion in the density around each electron. In this scheme the self-consistent potential in (A3.1) is given by

$$V = -e[\Phi_{ext} + (1 - G)\Phi_{ind}] \quad (A3.11)$$

which leads to a self-consistency equation

$$\Phi = \Phi_{ext} + v(\mathbf{q})\chi_0[\Phi_{ext} + (1 - G)\Phi_{ind}] \quad (A3.12)$$

from which (A3.10) is obtained.

In the RPA or standard SCFA, $G(\mathbf{q}, \omega) = 0$, yet the pair correlation function $g(\mathbf{r})$ becomes negative at small distances and the compressibility sum-rule is violated [2,4,16]. Reasonable approximations for $G(\mathbf{q}, \omega)$ can be found in [16,17]. For instance, in the Hubbard-approximation

$$G_H(\mathbf{q}, \omega) = \frac{1}{2} \frac{q^2}{q^2 + k_F^2}. \quad (A3.13)$$

In today’s ab initio calculations exchange and correlation effects can be taken into account within the local density approximation which, in most metals, leads to satisfactory results, yet with enormous numerical efforts, see e.g. [20,21,88].

A4. Bulk Loss-Function

To relate the inelastic electron scattering probability to the dielectric function we start from the work done by a particle moving parallel to the z-axis with constant velocity $\mathbf{v} = (0, 0, v_0)$ and impact vector $\mathbf{r}_0 = (x_0, y_0, 0)$. According to the Maxwell-equations (22) the electron charge distribution

$$\rho_{ext}(\mathbf{r}, t) = -e\delta(\mathbf{r} - \mathbf{v}t - \mathbf{r}_0) \quad (A4.1)$$

leads to longitudinal field components

$$D_\ell(\mathbf{q}, \omega) = \frac{2\pi ie}{q} \delta(\omega - \mathbf{q}_\parallel v_0) \exp(-i\mathbf{q}_\perp \mathbf{r}_0). \quad (A4.2)$$

For fast but nonrelativistic electrons, the reaction of the dielectric on the electron as well as contributions from \mathbf{E}_t and \mathbf{B} can be neglected. The work done per unit time by the electron is given by

$$\begin{aligned} \frac{dW}{dt} &= \int \mathbf{j}_{ext}(\mathbf{r}, t) \mathbf{E}_{ind}(\mathbf{r}, t) d^3\mathbf{r}, \\ &= -e\mathbf{v} \mathbf{E}_{ind}(\mathbf{v}t + \mathbf{r}_0, t), \\ &= - \int \frac{2i\pi e^2 \omega}{\epsilon_0 q^2} \left[\frac{1}{\epsilon_\ell(\mathbf{q}, \omega)} - 1 \right] \delta(\omega - q_\parallel v_0) \frac{d^3 q d\omega}{(2\pi)^4} \end{aligned} \quad (A4.3)$$

The real part of $\epsilon_\ell(\mathbf{q}, \omega)$ is an even function with respect to frequency and, therefore, it drops-out from (A4.3). As a result we obtain

$$\frac{dW}{dt} = \int \int \hbar\omega P(\mathbf{q}, \omega) \frac{d^3 q d(\hbar\omega)}{(2\pi)^4} \quad (A4.4)$$

with

$$P(\mathbf{q}, \omega) = \frac{2\pi e^2}{\epsilon_0 \hbar q^2} \text{Im} \left[- \frac{1}{\epsilon(\mathbf{q}, \omega)} \right] \delta(\hbar\omega - \hbar q_\parallel v_0). \quad (A4.5)$$

The loss-function $P(\mathbf{q}, \omega)$ can be interpreted as the rate for excitation of “photons” with energy $\hbar\omega$ and momentum q .

References

1. I. Langmuir, Proc. Nat. Acad. Sci **14**, 627 (1926).
2. D. Pines, *Elementary Excitations in Solids*, Benjamin (1964).
3. L. Marton, J.A. Simpson, H.A. Fowler, and N. Swanson, Phys. Rev. **126**, 182 (1962).
4. D. Pines and Ph. Nozieres, *The Theory of Quantum Liquids*, Benjamin (1966).
5. P.M. Platzman and P.A. Wolf, Solid State Phys., Suppl. 13, Academic (1973).
6. B. DiBartolo ed., *Collective Excitation in Solids*, Nato ASI Series B, vol 88, Plenum (1981).
7. H. Raether, *Excitations of Plasmons and Interband Transitions by Electrons*, Springer Tracts in Modern Physics, Vol. 88, Springer (1980).
8. S.E. Schnatterly, Solid State Physics, **34**, 275 (1979).
9. J. Fink, *Recent Developments in Energy-Loss-Spectroscopy*, Adv. in Electronics and El. Physics, Vol. 75, Academic Press, (1985).
10. N. Ashcroft and N.D. Mermin, *Solid State Physics*, Holt, Rinehart and Winston (1996).
11. D.M. Ceperley and B.J. Adler, Phys. Rev. Lett. **45**, 566 (1980).
12. F. Wooten, *Optical Properties of Solids*, Academic (1972).
13. L.V. Keldysh, D.A. Kirshnits, and A.A. Maradudin eds., *The dielectric function of condensed systems*, North Holland (1989).
14. a) J. Sprösser-Prou, A. vom Felde, and J. Fink, Phys. Rev. **B40**, 5799 (1989).
b) J. Sprösser-Prou, Diplom-Arbeit (1989), Institut für Nukleare Festkörperphysik, Forschungszentrum Karlsruhe (unpublished).
15. a) A. vom Felde, J. Fink, Th. Büche, B. Scheerer, and N. Nücker, Eur. Lett. **4**, 1037 (1987).
b) A. vom Felde, J. Sprösser-Prou, and J. Fink, Phys. Rev. **B40**, 1081 (1989).
16. P. Vashishta and K.S. Singwi, Phys. Rev. **B6**,875 (1972).
17. B. Dabrowski, Phys. Rev. **B34**, 4989 (1986).
18. M. Taut and K. Sturm, Sol. St. Comm. **82**, 295 (1992).
19. E. Lipparini, S. Stringari, and K. Takayanagi, J. Phys. Cond. Mat. **6**, 2025 (1994).
20. a) M. Kollwitz and H. Winter, J. Phys: Condens. Matter **7** 3153 (1995).
b) M. Kollwitz, Diplomarbeit, Institut für Nukleare Festkörperphysik, Forschungszentrum Karlsruhe (1994), unpublished.
21. F. Aryasetiawan and K. Karlson, Phys. Rev. Lett. **73**, 1679 (1994).
22. N. Nücker, U. Eckern, J. Fink and P. Müller, Phys. Rev. **B44**, 7155 (1991).
23. D. Pines, Can. J. Phys. **34**, 1379 (1956).
24. H., Fröhlich, J. Phys. **C1**, 544 (1968).
25. A. Pinczuk, Phys. Rev. Lett. **47**, 1487 (1981).
26. J. Ruvalds, Adv. Phys. **30**, 677 (1981).
27. F.C. Schaefer and R. v. Baltz, Z. Phys. **B69**, 251 (1987).
28. R.H. Ritchie, Phys. Rev. **106**, 874 (1957).
29. H. Raether, in *Physics of Thin Films*, Vol. 9, ed. by G. Hass, M.H. Francombe, and R.W. Hoffman, Academic (1977).
30. M. Cardona, Am. J. Phys. **39**, 1277 (1971).
31. F. Forstmann and R.R. Gerhardtts, *Metal Optics Near the Plasma Frequency*, Springer Tracts in Modern Physics, Vol 109, Springer (1986)
32. M. Born and E. Wolf, *Principles of Optics*, Pergamon (1959).
33. R. Fuchs and K.L. Kliewer, Phys. Rev. **B3**, 2270 (1971).
34. J. Zenneck, Ann. Phys. (Leipzig) **23**, 846 (1907); see: A. Sommerfeld, *Vorlesungen über Theoretische Physik*, VI, § 32, Leipzig (1966).
35. R.W. Wood, Phil. Mag. **4**, 396 (1902).
36. R.H. Ritchie, E.T. Arakawa, J.J. Cowan, and R.N. Hamm, Phys. Rev. Lett. **21**, 1530 (1968).
37. B. Fischer, N. Marschall, and H.J. Queisser, Surf. Sci. **34**, 50 (1973).
38. J. Bennett, Phys. Rev. **B1**, 203 (1970).
39. K.J. Krane and H. Raether, Phys. Rev. Lett. **37**, 1355 (1976).
40. F. Forstmann and H. Steuschke, Phys. Rev. **B17**, 1489 (1978).
41. K.D. Tsuei, E.W. Plummer, A. Liebsch, E. Pehlke, K. Kempa, and P. Bakshi, Surf. Sci. **247**, 302 (1991).
42. J. Harris and A. Griffin, Phys. Lett. **34A**, 51 (1971).
43. F. Flores and F. Garcia-Molinier, Sol. St. Comm. **11**, 1295 (1972).

44. P.J. Feibelman, Phys. Rev. Lett. **30**, 975 (1973). Progress in Surface Science, Vol 12, 287 (1982).
45. Ku-Ding Tsuei, E.W. Plummer and P. Feibelman, Phys. Rev. Lett. **63**, 2256 (1989).
46. S. Suto, K.-D. Tsuei, E.W. Plummer, and E. Burstein, Phys. Rev. Lett. **63**, 2590 (1989).
47. M. Rocca, M. Lazzarino, and M. Valbusa, Phys. Rev. Lett. **67**, 3197 (1991); **69**, 2122 (1992).
48. A. Liebsch, Phys. Rev. Lett. **71**, 1451 (1993).
49. W. Halperin, Rev. Mod. Phys. **58**, 533 (1986).
50. G. Mie, Ann. Phys. (Leipzig), **25**, 377 (1908).
51. J. Crowell and R.H. Ritchie, Phys. Rev. **172**, 436 (1968).
52. W. Ekhardt, Phys. Rev. **B32**, 1961 (1985); **B33**, 8803 (1986); **B36**, 4483 (1987).
53. F. Fujimoto and K. Komaki, J. Phys. Soc. Jap. **25**, 1679 (1968).
54. M. Barberan and J. Bausells, Phys. Rev. **31**, 6354 (1985).
55. R. v. Baltz, M. Mensch, and H. Zohm, Z. Phys. **B98**, 151 (1995).
56. R.B. Hall, Am. J. Phys. **31**, 696 (1963).
57. A.R. Melnyk and M.J. Harrison, Phys. Rev. Lett **21**, 85 (1968). Phys. Rev. **B2**, 835 (1970).
58. R.F. Egerton, *Electron Energy Loss Spectroscopy in the Electron Microscope*, Plenum (1986).
59. J.C. Ashley and T.L. Ferrell, Phys. Rev **B14**, 3277 (1976).
60. A. vom Felde, J. Fink, and W. Ekardt, Phys. Rev. Lett. **61**, 2249 (1988).
61. R. Manzke, G. Crezelius, and J. Fink, Phys. Rev. Lett **51**, 1095 (1983).
62. A. vom Felde, J. Fink, Th. Müller-Heinzerling, J. Pflüger, B. Scheer, and D. Kaletta, Phys. Rev. Lett. **53**, 922 (1984).
63. King-Sun David Wu and D.E. Beck, Phys. Rev **B36**, 998 (1987).
64. Ll. Serra, F. Garcias, J. Navarro, N. Barberan, M. Barranco, and M. Pi, Phys. Rev. **B46**, 9369 (1992).
65. M. Brack, Rev. Mod. Phys. **65**, 677 (1993).
66. H. Haberland, B. von Issendorff, Ji Yufeng, and Th. Kolar, Phys. Rev. Lett **69**, 3212 (1992).
67. K. Rademann, O. Dimopoulou-Rademann, M. Schlauf, U. Even, and F. Hensel, Phys. Rev. Lett. **69**, 3208 (1992).
68. C. Yannouleas, E. Vigezzi, and R.A. Broglia, Phys. Rev. **B47**, 9849 (1993).
69. R. Klauser et al. Surf. Sci. Lett. **255**, L557 (1991).
70. F. Stern, Phys. Rev. Lett. **18**, 546 (1967).
71. D. Heitmann, Surf. Sci. **170**, 332 (1986).
72. R.J. Wilkinson, C.D. Ager, T. Duffield, H.P. Hughes, D.G. Hasko, H. Ahmed, J.E.F. Frost, D.C. Peacock, D.A. Titchie, and G.A.C. Jones, J. Appl. Phys. **71**, 6049 (1992).
73. D. Olego, A. Pinczuk, A.C. Gossard, and W. Wiegman, Phys. Rev. **B26**, 7867 (1982).
74. E.L. Yuh, E.G. Gwinn, P.R. Pinsukanjana, W.L. Schaich, P.F. Hopkins, and A.C. Gossard, Phys. Rev. Lett. **71**, 2126 (1993).
75. M. Babiker, J. Phys. C **20**, 3321 (1987).
76. H. Shi and A. Griffin, Phys. Rev. **B44**, 11977 (1991).
77. E. Lopez Olazagasti, H. Coccoletzi, and W. Luiz Mochan, Sol. St. Comm. **78**, 9 (1991).
78. A. Griffin, Physica **C162-164**, 1427 (1989).
79. S.V. Pokrovsky and V.L. Pokrovsky, to be published
80. F. Bloch, Z. Phys. **81**, 363 (1933).
81. H. Jensen, Z. Phys. **106**, 620 (1937).
82. E.M. Lifschitz and L.P. Pitaevskii, *Physical Kinetics, Landau and Lifschitz Course on Theoretical Physics*, Vol 10, Pergamon (1981).
83. H. Ehrenreich and M.H. Cohen, Phys. Rev. **115**, 786 (1959).
84. S.L. Adler, Phys. Rev. **126**, 413 (1962).
85. N. Wiser, Phys. Rev. **129**, 62 (1963).
86. K. Sturm, Adv. Phys. **31**, 1 (1981).
87. N.D. Mermin Phys. Rev. **B1**, 2362 (1970).
88. Keun-Ho Lee and K.J. Chang, Phys. Rev. **B49**, 2362 (1994).